Received: 14 June 2023 | Accepted: 30 November 2023

DOI: 10.1111/jpy.13424

Phycological Society of America

RESEARCH ARTICLE

Convergent photophysiology and prokaryotic assemblage structure in epilithic cyanobacterial tufts and algal turf communities

Ethan C. Cissell | **Sophie J. McCoy**

Department of Biology, The University of North Carolina at Chapel Hill, Chapel Hill, North Carolina, USA

Correspondence
Ethan C. Cissell, Department of Biology, The University of North Carolina at Chapel Hill, Chapel Hill 27599, NC, USA.
Email: ecissell@unc.edu

Funding information
National Science Foundation, Grant/Award Number: 074012-520-044116; Florida "Protect Our Reefs" Grants Program, Grant/Award Number: POR_2020_03

Editor: M. Steffen

Abstract

As global change spurs shifts in benthic community composition on coral reefs globally, a better understanding of the defining taxonomic and functional features that differentiate proliferating benthic taxa is needed to predict functional trajectories of reef degradation better. This is especially critical for algal groups, which feature dramatically on changing reefs. Limited attention has been given to characterizing the features that differentiate tufting epilithic cyanobacterial communities from ubiquitous turf algal assemblages. Here, we integrated an in situ assessment of photosynthetic yield with metabarcoding and shotgun metagenomic sequencing to explore photophysiology and prokaryotic assemblage structure within epilithic tufting benthic cyanobacterial communities and epilithic algal turf communities. Significant differences were not detected in the average quantum yield. However, variability in yield was significantly higher in cyanobacterial tufts. Neither prokaryotic assemblage diversity nor structure significantly differed between these functional groups. The sampled cyanobacterial tufts, predominantly built by *Okeania* sp., were co-dominated by members of the Proteobacteria, Firmicutes, and Bacteroidota, as were turf algal communities. Few detected ASVs were significantly differentially abundant between functional groups and consisted exclusively of taxa belonging to the phyla Proteobacteria and Firmicutes. Assessment of the distribution of recovered cyanobacterial amplicons demonstrated that alongside sample-specific cyanobacterial diversification, the dominant cyanobacterial members were conserved across tufting cyanobacterial and turf algal communities. Overall, these data suggest a convergence in taxonomic identity and mean photosynthetic potential between tufting epilithic cyanobacterial communities and algal turf communities, with numerous implications for consumer-resource dynamics on future reefs and trajectories of reef functional ecology.

KEYWORDS
carbon, cyanobacteria, cyanobacterial mat, functional ecology, metabarcoding, metagenomics, *Okeania*, photosynthesis, refugia, turf algae

Abbreviations: ASV, amplicon sequence variants; CLR, centered-log ratio; DOC, dissolved organic carbon; LM, linear model; MAG, metagenome-assembled genome; PAM, pulse amplitude modulated; PAR, photosynthetically active radiation; TSS, total sum scaling.

INTRODUCTION

Coral reefs globally are experiencing shifts in benthic community structure toward the dominance of non-calcifying taxa, which can jeopardize the taxonomic and functional complexity necessary to provision desirable ecological and economic services by coral reef environments (Lester et al., 2020). Benthic cyanobacteria are increasingly reported in association with common trajectories of reef degradation, including the increase in cover of spatially discrete epipelic cyanobacterial mat communities, epilithic tufting cyanobacterial communities, and extensive blooms of benthic cyanobacteria (Albert et al., 2005; Cissell & McCoy, 2022a; de Bakker et al., 2017; de Ribeiro et al., 2022; Ford et al., 2017; Ford et al., 2018; Paul et al., 2005). The increasing dominance of conspicuous benthic cyanobacterial assemblages has been continuously linked to deleterious ecosystem-scale consequences from systemic biogeochemical changes, bloom toxicity, and increased competitive or pathogenic interactions with reef coral (Cissell et al., 2022, de Ribeiro et al., 2022, Puyana et al., 2019). As cyanobacterial dominance increases, it becomes increasingly important to understand how they are differentiated from current dominant benthic primary producers and to understand their contributions to reef functional ecology—notably their contributions to basal carbon cycling in reef environments.

Benthic algae and cyanobacteria are the dominant contributors to primary productivity and organic carbon production in coral reef ecosystems (Brocke et al., 2015; Mueller et al., 2014). Historically, this basal carbon flow has been driven by the photosynthetic activity of endosymbiotic dinoflagellates, fleshy macroalgal taxa, crustose coralline algae, and the structurally and compositionally heterogeneous functional habitat Epilithic Algal Matrix, which is dominated by filamentous turf algal communities (Odum & Odum, 1955). Turf algae often dominate reef primary productivity, contributing up to one-third of gross reef productivity (Klumpp & McKinnon, 1989; Tebbett & Bellwood, 2021). The contribution of turf algae to reef primary productivity is likely to only expand in the coming decades, with turf algal cover and productivity expanding dramatically on reefs globally in response to global change, alongside marked declines in coral cover (Jouffray et al., 2015; Smith et al., 2016).

Alongside a focus on turf algal contributions to carbon cycling, the contributions of general reef-associated cyanobacteria to primary productivity and reef carbon stoichiometry have also been relatively well studied. For example, endolithic cyanobacteria (especially euendolithic cyanobacteria such as *Hyella* spp., *Plectonema* spp., and *Mastigocoleus* spp.) are dominant contributors to carbon and carbonate cycling within the dead coral substrate, with endolithic carbon production comparable to that of scleractinian corals (Arp et al., 1999; Tribollet et al., 2006). However, relatively fewer studies have determined the specific contribution of these recently proliferating, conspicuous epipelic, and epilithic cyanobacterial aggregations, such as benthic cyanobacterial mats and cyanobacterial tufts. Benthic substrates dominated by cyanobacterial mats have been recently demonstrated to have higher rates of net primary productivity than substrates dominated by algal turfs (Webb et al., 2021), with potential interactive effects among local nutrient environment and mat productivity (Albert et al., 2005). Mat-building cyanobacteria can rapidly take up and utilize environmental nutrients relative to macroalgal competitors, likely exacerbating their contribution to reef productivity (den Haan et al., 2016). However, it was also recently demonstrated that benthic cyanobacterial mats, at least on Caribbean reefs, release a great deal of this fixed carbon back into their surrounding reef environment as Dissolved Organic Carbon (DOC) and thus act as net sources of DOC, especially during the night (Brocke et al., 2015; Mueller et al., 2022). This algal-derived DOC is more readily bioavailable to microbes and sponges on reefs and fuels inefficient carbon metabolism compared to coral-derived DOC, which can play a role in the expansion of opportunistic pathogens on reefs and contribute to overall reef microbialization (Haas et al., 2016; Silva et al., 2021). More studies that directly compare the photophysiology and microbial identity of these two simultaneously expanding groups across a broader geographic range will be critical to a better understanding of carbon cycling on future reefs.

Benthic cyanobacterial aggregations on reefs are complex consortia that can be built structurally by a few or many taxonomically distinct cyanobacterial members (Brocke et al., 2018; Cissell & McCoy, 2021; Echenique-Subiabre et al., 2015; Stuij et al., 2022). The dominant cyanobacterial component, primarily responsible for pioneering the cohesive structural matrix (Stal, 1995), is often complemented by a rich diversity of non-oxygenic autotrophs, heterotrophic bacteria, archaea, and viruses that contribute to overall community physiology, functional ecology, and emergent stability dynamics (Cissell & McCoy, 2021, 2022b, 2023a, 2023b; Stuij et al., 2022). Cyanobacteria, however, can also be predominant members of the prokaryotic assemblage within turf algal communities, alongside a dominance of Proteobacteria (predominantly Alphaproteobacteria), Bacterioidota, and Firmicutes (Barott et al., 2011; Hester et al., 2016). Indeed, shifts in turf composition toward higher cyanobacterial dominance can skew turf algal carbon cycling toward net DOC release (Mueller et al., 2022), which can contain cyanobacteria taxonomically similar to those known to be dominant mat-building cyanobacteria (Fricke et al., 2011). Few papers, however, have simultaneously examined the prokaryotic assemblage structure in benthic cyanobacterial aggregations and turf algae to define overlap and resolve

distinctions between the prokaryotic assemblage well—and namely the cyanobacterial component—of these two critical function groups well.

Here, we paired an in situ assessment of photophysiology with 16S rRNA gene metabarcoding to understand better how tufting benthic cyanobacterial communities compare to algal turfs in overall prokaryotic assemblage structure and their potential to contribute to benthic primary productivity in coral reef ecosystems. We further described the community structure of epilithic tufting cyanobacterial communities using shotgun metagenomic sequencing of bulk-extracted DNA to resolve community composition more fully in this important benthic functional group in the Florida Keys.

MATERIALS AND METHODS

Study site, photophysiology measurements, and field sampling

All field measurements and field sampling were conducted via SCUBA at Middle Sambo Reef (24.495167, −81.696500) within the Florida Keys National Marine Sanctuary on the Florida Keys Reef Tract offshore Florida, USA, on August 30, 2021. This work complied with Special Activity License SAL-21-2349-SR issued by the Florida Fish and Wildlife Conservation Commission and Florida Keys National Marine Sanctuary Research Permit FKNMS-2021-140 issued by the National Oceanic and Atmospheric Administration, Office of National Marine Sanctuaries. Benthic community composition at the sampling location on Middle Sambo Reef was assessed within photographs of 0.25 m^2 PVC photo quadrats ($n = 30$ quadrats). Photo quadrats were placed every 1 m along three 10-m transects placed haphazardly on the benthos at 3.3 m depth. Quadrats were never moved to select for hard substrate artificially and were always placed at every meter mark on each transect. Within CoralNet and under 50 randomly allocated points within each photo quadrat, benthic identity was manually assigned to one of 10 functional groups, comprised of the following: (1) Benthic Cyanobacterial Tufts (abbreviated BCTs in Appendix S1: Figure S1 in the Supporting Information), (2) Crustose Coralline Algae (CCA) + Turf, (3) Other Macroalgae, (4) Stony Coral, (5) *Millepora* spp., (6) *Palythoa* spp., (7) Sediment+Rubble, (8) Soft Coral, (9) Sponge, and (10) Unknown. Crustose coralline algae and turf algae were grouped into a single functional grouping because many CCA crusts present at this site were fouled with turf. The benthic community composition of these functional groups is presented in Figure S1.

Turf algae here is compositionally defined following previously presented standards (Connell et al., 2014; Hester et al., 2016) as epilithic algal aggregations built primarily by filamentous algae containing associated juvenile macroalgae, cyanobacteria, and an associated non-phototrophic (oxygenic) bacterial assemblage. The morphotype of the sampled turf algal communities here most closely resembles short productive algal turfs (Goatley et al., 2016), marked by low sediment loads and short conspicuous algal filaments. Epilithic benthic cyanobacterial tufts here are distinguished in name (perhaps only nominally) from previously described epipelic benthic cyanobacterial mats (e.g., Cissell & McCoy, 2021) because of their epilithic growth habitat and primarily vertically tufting, rather than horizontally spreading (i.e., comparatively restricted horizontal extent), morpho-anatomical growth habit. A more in-depth presentation of the utility of this subtle, formal distinction is given in the discussion of this manuscript. Cyanobacterial tufts were distinguished from turf algae during the in situ assessment of photophysiology and sampling primarily based on color, where cyanobacterial tufts were marked by a pronounced orange-brown pigmentation that was consistent throughout the cohesive structural matrix. Depending on the composition of the cyanobacterial assemblage, cyanobacterial tufts and mats can have vastly different colors and morphologies. A photograph of a tufting cyanobacterial community displaying the conserved macroscopic morphotype of the orange-brown tufts that were targeted and sampled in this study is given in Figure 1a and Appendix S1: Figure S2. Cyanobacterial tufts were additionally differentiated from turf algae in the field based on macroscopic habit, where turf contained primarily conspicuous vertically erect filaments and lacked a robust conspicuous structural matrix. In contrast, cyanobacterial tufts were marked by a structurally cohesive and conspicuous matrix consisting primarily of horizontally arranged filaments with sparse vertically tufting cyanobacterial filaments.

To quantify ambient concentrations of inorganic $NO_x^{(-y)}$ species (NO_3^-, NO_2^-), NH_4^+, and inorganic PO_4^{-3} at this study site, seawater samples ($n = 4$) were collected haphazardly from immediately above the benthos-seawater interface (3.3 m depth) in sealable, triple acid-washed 75-mL LDPE sample vials (Thermo Scientific). These samples were immediately filtered at the surface using pre-sterilized 0.2-μm PES membrane syringe filters (Gelman Sciences), stored on ice in the dark during transport and at −20°C upon arrival at Florida State University. $NO_x^{(-)}$ species were subsequently quantified using spectrophotometric analysis that leveraged a sequential Griess reaction with the addition of VCl_3 (García-Robledo et al., 2014). NO_3^- and NO_2^- were detected with a 0.2 μM detection limit. Finally, PO_4^{-3} concentrations were quantified using a spectrophotometric method following the formation of molybdenum blue complex from the reaction of orthophosphate with ammonium molybdate in the presence of sulfuric acid (Habibah et al., 2018). PO_4^{-3}

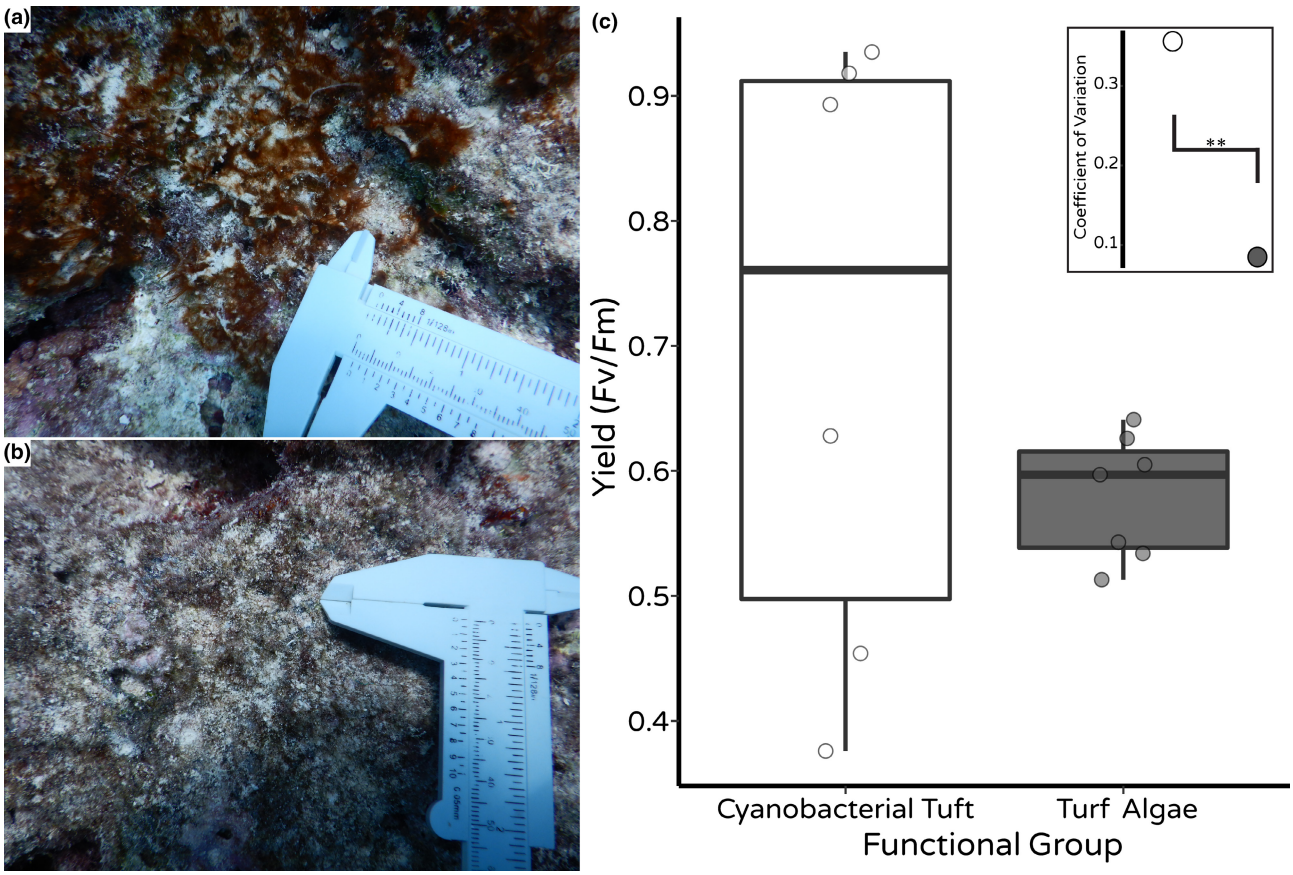

FIGURE 1 Only the variability in yield differs between sampled groups. Photographs of (a) representative benthic cyanobacterial tufts and (b) turf algal communities sampled in this study. (c) Boxplots showing the distribution of in situ instantaneous photosynthetic yield measurements grouped by assessed benthic functional group (benthic cyanobacterial tufts, $n=6$, and turf algae, $n=7$). The mean of measured yield did not significantly differ between groups (Welch's t-test; $t=1.168$, $df=5.3$, $p=0.29$). The inset plot (box in the upper-right of the main plot) presents a dot plot of the coefficient of variation (CV) in these quantum yield measurements grouped by the assessed benthic functional group. The coefficient of variation in yield was significantly higher in benthic cyanobacterial tufts than in turf algae (Asymptotic test: $D=8.45$, $p=0.004$; Signed-likelihood ratio test: $L=7.76$, $p=0.005$). [Color figure can be viewed at wileyonlinelibrary.com]

concentrations were quantified with a 0.2 μM detection limit. The measured environmental concentrations of each of these nutrients are presented in Appendix S1: Table S1.

A DIVING-pulse amplitude modulated (PAM) underwater fluorometer (Waltz) was used to assess in situ instantaneous maximum quantum yield (hereafter yield) of samples of epilithic tufting cyanobacteria ($n=6$) and turf algae ($n=7$) of similar vertical heights (~1 cm vertical relief) located at 3–4 m depth via quantification of basal (F_0) and maximal fluorescence (F_m) of dark-adapted material. Though $n=8$ samples were targeted from each group, yield measurements failed on two tufting cyanobacterial samples and one turf algal sample, for a final datasets of $n=6$ yield measurements for cyanobacterial tufts and $n=7$ samples for turf algal communities. Targeted cyanobacterial tufts all had consistent morphological appearance (Figure 1a, Figure S2). Sampling carefully targeted areas completely devoid of underlying or entangled macroalgal thalli (primarily from *Dictyota* spp.) to avoid any confounding effects of macroalgal presence. Yield is given as F_v/F_m, where $F_v=F_m-F_0$. Samples were each placed in a 20 min dark adaptation period prior to photophysiological assessment using 5 cm^2 pieces of weighted aluminum foil that completely shielded the underlying samples from intruding photosynthetically active radiation (PAR). Following this dark adaptation period, F_0 and F_m were determined from a single saturating light pulse. Ambient PAR during photophysiology measurements was assessed at a fixed point at 3.3 m depth using a calibrated submersible PAR logger (Odyssey; serial number 13046) set to a scanning interval of 30 s ($n=287$ total scans). The mean calibrated PAR at the site at 3.3 m depth across the sampling period was 321.3 $\mu mol \cdot m^{-2} \cdot s^{-1} \pm 114.2$ *SD*.

Samples of approximately 0.5 mL volume each were collected immediately after each respective yield quantification using sterile forceps, carefully targeting the biomass for which yield was assessed. For benthic cyanobacterial tufts, this sampling targeted the entirety of the structural matrix (i.e., all vertical layers connected within a cohesive structural matrix) that was observed directly beneath the PAM sensor. For turf algae, this

sampling targeted the conspicuous filamentous matrix comprising the turf, which was removed until only the bare underlying substrate remained (i.e., removing all filamentous algae and associated community). Notably, this sampling of turf algae and cyanobacterial tufts would include trapped detritus in the community matrix and detrital-associated prokaryotic assemblages. Collected samples were immediately (post-dive) preserved in 2× their volume of DNA/RNA Shield (Zymo) and stored on ice in the dark during marine transport, at −20°C while at the field station (<24 h) and at −80°C upon arrival back at Florida State University until DNA extractions and library preparation.

DNA extractions, library preparation, and metabarcoding

Microbial genomic DNA was extracted from samples following previously presented protocols (Cissell & McCoy, 2021). Briefly, bulk DNA extraction proceeded on 0.25 mL of each of the homogenized samples using a combination of physical (variable glass beads) and chemical lysis using the E.Z.N.A Soil DNA Kit (Omega) following the manufacturer's protocol, and extracted DNA was eluted in 50 μL of elution buffer. Using a Covaris ME220 Focused-Ultrasonicator (Covaris Inc), eluted DNA was sheared to an average length of 524 bp (shotgun) or 623 bp (amplicon).

For metabarcoding, the V3–V4 hypervariable regions of the bacterial 16S rRNA gene were amplified by PCR using the bacterial-specific primers 341F: 5′-CCT ACG GGN GGC WGC AG-3′ and 805R: 5′-GAC TAC HVG GGT ATC TAA TCC-3′ (Herlemann et al., 2007; Klindworth et al., 2013). Metabarcoding was performed on both functional groups (cyanobacterial tufts: $n = 8$ and turf algae: $n = 8$). Polymerase chain reactions were carried out on 2.5 μL DNA (5 ng · μL^{-1} concentration), 5 μL each from amplicon primers, and 12.5 μL KAPA HiFi HotStart ReadyMix (25 μL total reaction volume per sample) using the following annealing conditions: 95°C for 3 min followed by 25 cycles of 95°C for 30 s, 55°C for 30 s, 72°C for 30 s, followed by 72°C for 5 min. Subsequent purification of amplicons (removal of free primers and primer dimers) was carried out using the AMPure XP magnetic bead protocol. Finally, dual indices and Illumina sequencing adapters were attached following the Nextera XT Index Kit protocol (PCR Conditions: 95°C for 3 min, eight cycles of 95°C for 30 s, 55°C for 30 s, 72°C for 30 s, 72°C for 5 min), followed by another round of library clean-up with AMPure XP beads. Libraries were diluted, pooled equimolar, and checked using Bioanalyzer and KAPA qPCR before submission for sequencing.

Libraries for shotgun metagenomic sequencing were prepared using the NEBNext UltraII DNA Library Prep Kit for Illumina (New England Biolabs) following the manufacturer's protocol with five cycles of PCR amplification and dual-indexing primers. Shotgun metagenomic libraries were only prepared from cyanobacterial tuft samples ($n = 2$). Qubit DNA HS reagents were used to quantify libraries initially, and Bioanalyzer 2100 High Sensitivity DNA Assay was used to check libraries for size and artifacts. To determine the molar quantity of each library, KAPA qPCR assay (KAPA Biosystems) was used. Libraries were diluted, pooled equimolar, and again checked using Bioanalyzer and KAPA qPCR before submission for sequencing. All samples (including both full shotgun and 16S rRNA gene amplicon libraries) were submitted for sequencing at Novogene on an Illumina NovaSeq 6000 using paired-end 150 bp chemistry (300 cycle kit). This sequencing generated a total of ~1.1 billion reads across all samples (Appendix S1: Table S2). These sequence data have been submitted to the NCBI sra database, accessible under BioProject accession number PRJNA983846.

Analysis of metabarcoding sequences

Demultiplexed, raw, paired-end metabarcoding reads were initially quality trimmed to a Phred quality score threshold of 20 and a minimum length threshold of 100 bp, and adapter sequences were removed using TrimGalore version 0.6.6 (with Cutadapt version 1.18). Amplicons passing these initial quality control steps were inspected using FastQC version 0.11.9. Reads were subsequently filtered using error expectation trimming implemented in DADA2 version 1.26.0 (Callahan et al., 2016), allowing for a maximum of two expected errors per read and a maximum of zero Ns. Reads were not truncated for length at this quality control step because the analysis of plots of base quality (Phred) against cycle suggested that no additional explicit positional trimming was necessary. Reads statistics from before and following these quality control steps are presented in Table S2. Cyanobacterial tuft sample C10 was removed from downstream analyses because over 99% of all reads in this read set were removed following quality control, leaving a total of $n = 7$ metabarcoding samples from cyanobacterial tufts and $n = 8$ samples from turf algae. Following quality control, all read sets were randomly subset (using Seqtk release 1.3; identical seeds) to 200,000 reads per sample to improve the computational efficiency of downstream error model construction. These reduced reads sets were used as inputs to train modified parametric error models from 8e+05 reads (~1e+08 bases) from forward and reverse read sets. Monotonicity was enforced in the modified error models fit with modified loess weighting structures and spans to account for this dataset's inherent binning of quality scores. Original full quality-controlled read sets were then randomly subset to 1,000,000 reads per sample (for computational efficiency), and

these larger subsets were subsequently used as inputs in DADA2 to cluster and retrieve de novo Amplicon Sequence Variants (ASVs) based on the previously trained error models. Forward and reverse read mate pairs were concatenated to obtain a merged pool of denoised sequences (i.e., justConcatenate = TRUE). Concatenation of non-overlapping reads was recently demonstrated to outperform subsetting the data to only forward read sets in reconstructing community composition (including taxonomic assignment) from amplicon sequencing data (Dacey & Chain, 2021). Chimeric ASVs were then inferred and removed from the resulting concatenated denoised variant table. Taxonomy was assigned to ASV read pairs using a naive Bayesian method with the Silva Project's nr99 database release 138.1 (Quast et al., 2012) as implemented by the RDP Classifier (Wang et al., 2007), which has been reported to be more robust for concatenated, non-merged reads (Abdala Asbun et al., 2020). Briefly, bootstrapped *k*-mer profiles (from all possible 8-mers) from queried sample ASVs were repeatedly matched to *k*-mer profiles in the Silva training set (positionally unaware) to establish a consensus taxonomic inference (from bootstrap confidence) for query sequences, retaining those assignments at each taxonomic hierarchy that exceeded a bootstrap confidence value of 40. The resulting ASV Biom table was subsequently filtered for likely artifacts by removing those reads that could not be assigned at least to the rank of Phylum (e.g., Phylum = NA). Reads assigned as Chloroplast, Mitochondria, or eukaryotic DNA were removed at this step. Rarefaction curves were constructed on the filtered datasets and suggested that the filtered AVS well recapitulated the diversity of the underlying community (each sample reached approximate saturation; Appendix S1: Figure S3). Downstream inference proceeded on a total of 346,672 reads (mean 23,111 ± 3483 *SD* reads per sample).

Phylogenetic reconstruction from metabarcoding sequences

A multiple sequence alignment was performed on all filtered ASVs assigned to the phylum Cyanobacteria by the RDP Classifier with a similarity-based alignment method implemented in MAFFT version 7.310 (Katoh & Standley, 2013). The alignment proceeded using an FFT-NS-i method with progressive refinement across two guide trees. A maximum likelihood phylogeny with branch support values was inferred using the resulting multiple sequence alignment with IQ-Tree version 5 (Minh et al., 2020) using a TVM + F + R4 model inferred as the optimal using a Bayesian information criterion model selection approach implemented in *ModelFinder* (Kalyaanamoorthy et al., 2017). Tree construction proceeded from 98 parsimony candidate trees using 1500 bootstrap approximation replicates. A tree-based agglomeration was applied to collapse tree leaves on the consensus phylogenetic tree at a threshold cophenetic distance of 0.5 on the original hierarchical clustering of the distance matrix.

Read-based analysis of shotgun metagenomes

Shotgun sequencing quality control proceeded similarly to previously reported methods (Cissell & McCoy, 2021). Demultiplexed, raw paired-end DNA reads had adapter sequences removed and were quality trimmed to a Phred quality score threshold of 25 and minimum length threshold of 100 bp using TrimGalore version 0.6.6 (with Cutadapt version 1.18). Contamination from human sequences was removed via end-to-end alignment of our reads against a soft-masked version of the human genome (HG38; patch release 13 [2019-02-28], GenBank Accession#: GCA_000001405.28) using Bowtie2 version 2.3.4.1 (Langmead & Salzberg, 2012) with the *-very-sensitive* flag (-D 20; -R 3; -N 0; -L 20; -I S, 1, 0.50), retaining unaligned reads (>>99.99% of reads retained; Table S2). The initial and final (following quality control) quality of reads was assessed using FastQC version 0.11.9. To estimate the coverage of the actual underlying community diversity our sequencing effort recovered, we used a read *k*-mer redundancy estimate implemented in *Nonpareil 3* version 3.304 (RodriguezR et al., 2018) on 31-mers pulled from a query size of 10,000 reads with 1024 sub-samples on each forward read set (Appendix S1: Figure S4, Table S3).

Read-based taxonomic profiles of quality-controlled paired-end metagenomic reads were generated using two complementary approaches: protein-based (translated reads) lowest common ancestor (LCA) lineage inference and clade-specific marker gene-based inference. This protein-sequence-based inference was favored over *k*-mer nucleotide-based inference because it has previously shown higher sensitivity and recall in annotating environmental datasets, overall providing higher taxonomic resolution with fewer erroneous alignments (Tovo et al., 2020). Reads were translated into amino acid sequences and matched against the NCBI nr protein database, including microbial eukaryotes (updated 2021-02-24) as implemented in Kaiju version. 1.8.2 (Menzel et al., 2016), retaining alignments that produced an e-value of 0.05 or less. A 0.1% relative abundance threshold was set to reduce the influence of false-positive taxonomic predictions resulting from this alignment-based method. Shotgun metagenomic-derived translation-resolved community composition was assessed from a total of 225,505,019 read-pair alignments to at least family level (68.2% of all read pairs). Read-based composition inferred from Kaiju is

presented as total sum scaling (TSS) values normalized to the total number of classified sequences in the sample (i.e., excluding unknown sequence counts).

Read-based taxonomic profiles were additionally generated using an alignment-based protocol against the CHOCOPhlAn single-copy marker gene database release 2021–03 (version Jan21) implemented in MetaPhlAn 4 version 4.0.3 (Blanco-Miguez et al., 2022). Briefly, Bowtie2 was used to map all quality-controlled read pairs (concatenated; mate information not retained) against the marker gene catalog curated from sequence-defined species-level genome bins (CHOCOPhlAn SGB). The coverage of each marker from the resulting alignment profile was calculated, and the robust average of the entire clade's coverage was subsequently calculated, normalized across detected clades (including unclassified), and retained as the final clade coverage value. A total of 21.4% and 22.4% of all reads could be successfully aligned against a species-level taxonomic marker gene in samples SC2 and SC3, respectively, using this single-copy marker gene-based approach. Abundance values (as above) are presented as TSS values normalized to the total number of classified sequences in the sample (i.e., excluding unknown sequence counts).

Assembly-based analysis of shotgun metagenomes

Quality-controlled metagenomic reads were assembled and scaffolded de novo using the IDBA-UD assembler version 1.1.3 (Peng et al., 2012), retaining scaffolds equal to or exceeding 1.5 kbp in length. The quality of the resulting assembly was assessed using *METAQUAST* version 5.0.2 (Appendix S1: Table S4; Gurevich et al., 2013). Scaffolds were binned unsupervised using *Metabat2* version 2.15 (Kang et al., 2019), *Maxbin2* version 2.2.7 (Wu et al., 2016), and *VAMB* version 3.0.2 (Nissen et al., 2021), with the default parameters used for each respective binning algorithm. *DasTool* version 1.1.2 was used to create a quality-controlled consensus bin set, retaining a total of 113 bins. The quality of this bin set was manually evaluated with outputs of *CheckM* version 1.1.3 (Parks et al., 2015), and bins with contamination ≥10% and completeness ≤60% were discarded. A total of 103 bins were retained that met these quality evaluation criteria and were defined as medium- to high-quality Metagenome-assembled genomes (MAGs; Bowers et al., 2017). Metagenome-assembled genomes that were retained were dereplicated at 95% global identity using *dRep* version 3.2.0 (Olm et al., 2017). *FastANI* version 1.32 (Jain et al., 2018) was used to perform the pairwise computation of the total average nucleotide identity across MAGs of interest. Coverage of each MAG was obtained by extracting high-quality mapping counts from global end-to-end alignments performed with Bowtie2 using *CoverM* version 0.6.1. The relative abundances of MAGs are given as TSS values normalized to the total mapped reads from each sample.

The taxonomic lineage of MAGs was assigned using the Genome Taxonomy Database (GTDB) taxonomy, assessed using *GTDB-Tk* version1.5.0 (Chaumeil et al., 2019) against release 06-RS202 of the GTDB. A maximum-likelihood phylogenomic tree with branch support values was inferred using the multiple sequence alignment of 120 bacterial marker genes (5037 amino acid sites) from *GTDB-Tk* with IQ-Tree using a Q.pfam+R8 model inferred as the optimal using a Bayesian Information Criterion model selection approach implemented in *ModelFinder*. Tree construction proceeded from 98 parsimony candidate trees using 1500 bootstrap approximation replicates. The consensus phylogenomic tree was visualized using *Itol* version 5 (Letunic & Bork, 2021).

Secondary/specialized metabolite biosynthesis gene clusters were identified on dominant MAGs annotated as phylum Cyanobacteria using BLAST+ and HMMer 3 searches implemented in *antiSMASH* version 6.0.0 (Blin et al., 2021).

Statistical analyses

All statistical analyses and data visualization were conducted using the R version 4.2.2 programming language within RStudio 2022.07.2 Build 576, Spotted Wakerobin. A Welch's *t*-test was used to compare the mean yields of the sampled tufting cyanobacteria and turf algal communities. Residuals were visually checked for normality. Significant differences in the coefficient of variation (CV) of yield measurements between functional groups were assessed using an asymptotic test following protocols presented in Feltz and Miller (1996) and using a modified signed-likelihood ratio test following protocols presented in Krishnamoorthy and Lee (2014).

All statistical analyses on sequencing data proceeded using the 16S rRNA gene amplicon sequencing data. No formal statistical analyses were performed on the generated shotgun metagenomic data. Alpha diversity metrics—including Chao1, Shannon-Weiner diversity, and Pielou's Evenness—were calculated from the filtered ASV count data grouping by sample type (i.e., Cyanobacterial Tuft vs. Turf Algae) using R::*phyloseq* version 1.42.0 (McMurdie & Holmes, 2013). Significant differences between sample types in alpha diversity metrics were assessed using pairwise Wilcoxon Rank Sum Tests with Bonferroni corrections. Differences in beta diversity between sample types were visualized using Non-metric Multidimensional Scaling (NMDS) based on an Aitchison dissimilarity matrix built from Centered-Log Ratio (CLR)-transformed ASV-level count

data. To ensure a proper matrix transformation, the input matrix for calculating Aitchison dissimilarity had all zero counts replaced using a pseudocount calculated as min(*count*) 2^{-1}. Clustering by sample type (among group variability) was assessed from the calculated Aitchison dissimilarity matrix using permutational multivariate analysis of variance (PERMANOVA) run with 999 permutations. The homogeneity of multivariate dispersion among samples from cyanobacterial tufts and turf algae was assessed and verified using *vegan::permutest.betadisper*, run using 999 permutations. Differential abundance analysis was then used to determine ASV-specific patterns differentiating turf algal and cyanobacterial tuft samples. ANOVA-like differential expression (*ALDEx2*; Fernandes et al., 2013) version 1.30.0 analysis was used with CLR-transformed ASV count data as inputs. A combination of effect size and median CLR transformed abundance difference was preferred to traditional *p*-value-based inference to establish a more meaningful and interpretable threshold of differential abundance. ANOVA-like differential expression calculates a non-parametric effect size estimate of between-group differences based on median standardized differences in group distributions (vectorized). A combination threshold of (1) effect size with an absolute value exceeding 0.6 and (2) a median difference in abundance exceeding an absolute value of 3.5 was used to assign significance to these abundance data. No ASVs were detected to be significantly differentially abundant under a more traditional $p < 0.05$ alpha value threshold following Benjamini-Hochberg corrections (from Welch's *t*-tests and Wilcoxon rank tests).

Community composition data were then subset to only include those ASVs assigned to the phylum Cyanobacteria. Significant differences between functional groups in alpha diversity metrics calculated from this cyanobacteria subset were assessed using pairwise Wilcoxon rank sum tests with Bonferroni corrections. Differences in beta diversity between functional groups were visualized using principal coordinates analysis (PCoA) based on a weighted UniFrac dissimilarity matrix (phylogenetic distances retrieved from the inferred consensus phylogenetic tree of all cyanobacterial ASVs).

The relationships between different calculated sample alpha diversity metrics (from metabarcoding) and in situ yield were assessed by fitting a series of ordinary least squares regressions, treating each alpha diversity metric individually as linear predictors of the numeric response variable *yield*. The conformity of residual structures to model assumptions was assessed graphically from model residual diagnostic plots produced using *R::DHARMa* version 0.4.6. These regressions were fit using diversity metric values calculated on the full ASV dataset from each sample and on subset datasets considering only the diversity of those ASVs assigned as phylum Cyanobacteria. The association of in situ yield with total prokaryotic assemblage structure was assessed using *vegan::envfit* to calculate a linear trend surface for yield (*p*-value assessed permutationally from 999 permutations) by fitting the vector of sample yields as a dependent variable against the ordination scores calculated from an NMDS based on an Aitchison dissimilarity matrix built from CLR-transformed ASV-level count data subset to only include those samples that possessed an associated in situ yield measurement.

RESULTS

Overview of study site

The sampled section of Middle Sambo Reef was dominated by carbonaceous substrate covered with crustose coralline algae and algal turf communities (CCA + Turf; mean cover = 0.54 ± 0.04 *SE*; Figure S1). Conspicuous benthic cyanobacterial communities made up a small fraction of the benthic community at this site (mean cover = 0.01 ± 0.003 *SE*) and were dominated by tufting cyanobacterial communities morphotypically similar to those sampled in this study. The benthic sessile invertebrate community was co-dominated by members of the order Alcyonacea (soft corals; primarily *Gorgonia ventalina*) and the zoanthid *Palythoa caribaeorum*. The measured total NO_x ($NO_3^- + NO_2^-$) at this site was 0.552 μM ± 0.231 μM (mean ± *SD*). Phosphate concentrations were below 0.2 μM in all samples (Table S1).

Variability in quantum yield differs between functional groups

We quantified the in situ photosynthetic yield of tufting cyanobacterial communities ($n = 6$) and turf algal communities ($n = 7$) to better understand the functional photophysiology of these two abundant benthic functional groups. The mean maximum yield did not significantly differ between these epilithic functional groups (Welch's *t*-test; $t = 1.168$, $df = 5.3$, $p = 0.29$), with a mean yield for cyanobacterial tufts at 0.70 ± 0.25 *SD* and a mean yield at 0.58 ± 0.05 *SD* for turf algal communities (Figure 1). While the mean yield did not significantly differ between these groups, the within-group variability (from the CV) of yield measurements was significantly higher in cyanobacterial tufts than in turf algae (Asymptotic test: $D = 8.45$, $p = 0.004$; Signed-likelihood ratio test: $L = 7.76$, $p = 0.005$; Figure 1). The CV of yield measurements was 0.356 and 0.085 for cyanobacterial tufts and turf algal communities, respectively (Figure 1). Photosynthetic yield in cyanobacterial tufts ranged from 0.376 to 0.935 while yield in turf algal communities ranged from 0.513 to 0.641.

Overview of the metabarcoding-resolved prokaryotic assemblage structure in sampled cyanobacterial tufts and turf algal communities

Amplicon sequencing of the 16s rRNA gene using universal bacterial-specific primers of collected cyanobacterial tuft ($n=7$) and turf algal ($n=8$) communities recovered a total of 23,050 unique ASVs across all samples. The recovered ASVs spanned 14 and 13 unique bacterial and archaeal phyla from cyanobacterial tufts and turf algae, respectively (a total of 16 unique phyla recovered across both functional groups; 10 unique bacterial and six unique archaeal phyla). Metabarcoding data revealed that both benthic functional groups were overwhelmingly dominated by ASVs belonging to the phylum Proteobacteria (20,087 total unique ASVs; Cyanobacterial Tuft: 83.5% ± 1.31% *SE*; Turf Algae: 83.2% ± 1.08% *SE* TSS relative abundance) and Firmicutes (1707 total unique ASVs; Cyanobacterial Tuft: 10.9% ± 0.55% *SE*; Turf Algae: 10.7% ± 0.54% *SE* TSS relative abundance). Amplicon sequence variants belonging to the phylum Cyanobacteria were not well represented in this metabarcoding dataset (281 total unique ASVs; Cyanobacterial Tuft: 1.51% ± 0.27% *SE*; Turf Algae: 1.03% ± 0.13% *SE* TSS relative abundance). Similar low recovery of cyanobacterial taxa using universal bacterial 16S rRNA gene primer sets is well documented in the literature (e.g., recently by Kang et al., 2022), making the low cyanobacterial recovery in this particular universal amplicon dataset unsurprising.

Amplicon sequence variants in this dataset were poorly annotated below phylum-level taxonomic annotation, likely owing to a combination of technical (non-overlapping read pairs) and biological (from the novelty of these environmental sequences) bases. A total of 79.2% ± 1.12% *SE* or 78.6% ± 1.30% *SE* of ASVs (from relative abundance; 17,361 total unique ASVs) were unclassified at the level of taxonomic class from the cyanobacterial tuft and turf algal samples, respectively. From those ASVs for which class-level taxonomy could be well resolved, both cyanobacterial tufts and turf algal samples were dominated by members of the Alphaproteobacteria (3868 total unique ASVs; Cyanobacterial Tuft: 13.0% ± 0.67% *SE*; Turf Algae: 13.1% ± 0.78% *SE* TSS relative abundance) and Bacilli (626 total unique ASVs; Cyanobacterial Tuft: 2.71% ± 0.26% *SE*; Turf Algae: 2.81% ± 0.24% *SE* TSS relative abundance; Appendix S1: Figure S5). A total of three of the top 10 most abundant (from TSS relative abundance) unique individual ASVs were shared between the two functional groups, with the top two most abundant ASVs being identical between the groups (Table 1). These top 10 most abundant ASVs across

TABLE 1 Classification of the 10 most abundant ASVs from each benthic functional group.

Benthic group	ASV ID	Relative abundance mean (%)	Relative abundance *SD* (%)	Lowest assigned taxonomy
Cyanobacterial tuft	ASV63	1.38	0.33	Firmicutes
	ASV134	0.90	0.47	Proteobacteria
	ASV606	0.66	1.09	Proteobacteria
	ASV288	0.66	0.35	Firmicutes
	ASV347	0.43	0.33	Firmicutes
	ASV545	0.43	0.68	Alphaproteobacteria
	ASV609	0.42	0.36	Proteobacteria
	ASV1090	0.39	0.49	Proteobacteria
	ASV1290	0.36	0.53	Proteobacteria
	ASV481	0.36	0.49	Proteobacteria
Turf algae	ASV63	1.30	0.47	Firmicutes
	ASV134	0.79	0.34	Proteobacteria
	ASV305	0.69	1.11	Proteobacteria
	ASV403	0.64	1.09	Firmicutes
	ASV435	0.57	0.67	Alphaproteobacteria
	ASV453	0.55	0.62	Alphaproteobacteria
	ASV347	0.46	0.24	Firmicutes
	ASV756	0.39	0.63	Bacilli
	ASV888	0.37	0.48	Proteobacteria
	ASV844	0.36	0.37	Halobacterota

Note: Provided is the identity of the broad sampled functional group (Benthic Group), the identifier of each unique ASV (ASV ID), the mean TSS-transformed relative abundance of each ASV across all samples when grouped by benthic functional group expressed as a percent (Relative Abundance Mean, %), the standard deviation in the relative abundance of each ASV across all samples when grouped by benthic functional group expressed as a percent (Relative Abundance *SD*, %), and the lowest assigned taxonomy of each ASV. The presented ASVs are ordered from most to least abundant within each functional group.

both groups were consistently dominated by members of the Firmicutes and Proteobacteria, notably those belonging to the Alphaproteobacteria. A complete graphical overview of the bacterial assemblage structure aggregated at the level of both taxonomic phylum and taxonomic class and grouped within the sampled benthic functional habitats is presented in Figure S5.

Cyanobacterial tufts and algal turfs have convergent prokaryotic assemblage diversity and structure and share dominant cyanobacterial taxa

A suite of alpha diversity metrics that resolve sample richness, evenness, and their combination was calculated for each sample to understand better diversity patterns in the sampled epilithic benthic functional groups as determined from 16S rRNA gene metabarcoding data. The recovered prokaryotic assemblages did not vary significantly between cyanobacterial tufts and turf algae in richness (Chao1; PWRST, $p = 0.34$), diversity (Shannon-Weiner; PWRST, $p = 0.87$), or evenness (Pielou's Index; PWRST, $p = 0.072$; Figure 2). The mean number of observed ASVs was 1677 ± 164.6 *SD* and 1844 ± 359.2 *SD* in the cyanobacterial tuft and turf algal samples, respectively (Figure 2). The mean richness was 1722 ± 172.8 *SD* in cyanobacterial tufts and 1896 ± 382.2 *SD* in turf algae. The mean Shannon diversity index value was 6.57 ± 0.15 *SD* in cyanobacterial tufts and 6.56 ± 0.19 *SD* in turf algae. The mean evenness of cyanobacterial tuft samples was 0.89 ± 0.01 *SD* and 0.87 ± 0.01 *SD* in turf algal samples.

The overall structure of the prokaryotic assemblage at the ASV level also did not significantly differ between the sampled cyanobacterial tufts and turf algal communities, with no significant clustering of community structure by benthic group (PERMANOVA, $k = 2$, stress = 0.155, $F = 0.999$, $p = 0.417$, $r^2 = 0.07$; Figure 3a). A compositional data-aware differential abundance analysis (based on CLR-transformed abundance data) was subsequently applied to the dataset to resolve ASV-specific differences in the composition of the resolved prokaryotic assemblage in these benthic functional groups. A total of 19 ASVs were detected to be significantly differentially abundant (significance threshold described in detail above in Materials and Methods: Statistical analyses) between cyanobacterial tuft and turf algal communities (Figure 3b). Thirteen of those ASVs were significantly more abundant in cyanobacterial tuft samples than in turf algal samples,

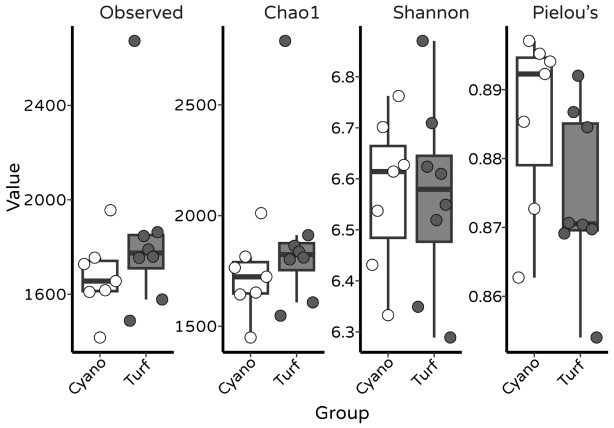

FIGURE 2 Community diversity does not differ between cyanobacterial tufts and turf algae. Boxplots showing the distribution of total observed ASV counts and different calculated alpha diversity metrics from metabarcoding of cyanobacterial tufts and turf algae. None of the calculated diversity metrics significantly differed between the functional groups, including richness (Chao1; PWRST, $p = 0.34$), diversity (Shannon-Weiner; PWRST, $p = 0.87$), or evenness (Pielou's Index; PWRST, $p = 0.072$).

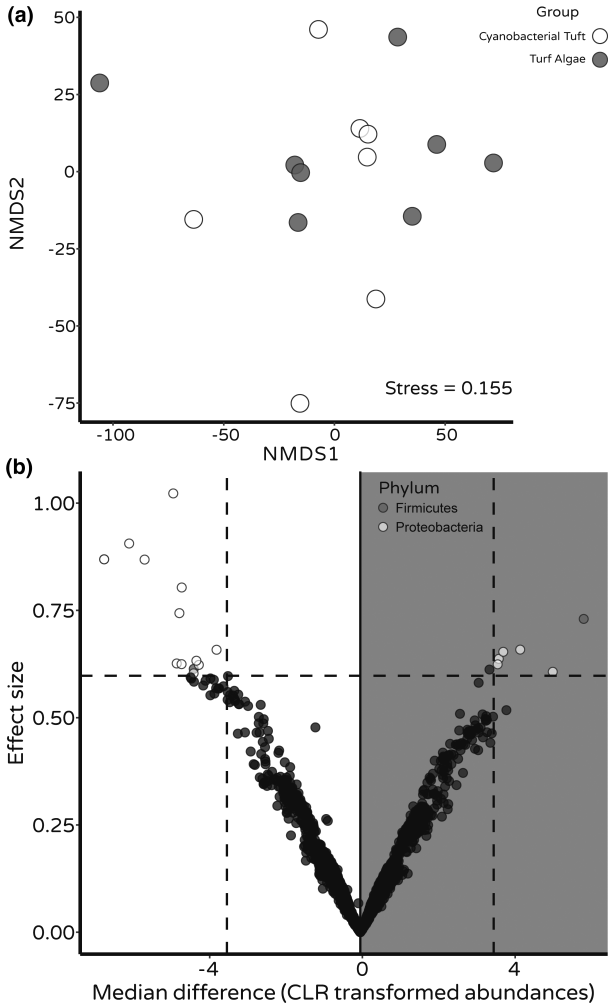

FIGURE 3 Community structure does not differ between cyanobacterial tufts and turf algae. (a) NMDS ordination based on Aitchison dissimilarity index of clr-transformed ASV-level count data displaying no significant clustering by functional group ($p = 0.442$, $r^2 = 0.07$). Samples are represented as individual points. (b) Volcano plot showing ASVs (individual points) that are differentially abundant between functional groups. The phyla for those ASVs that are differentially abundant are encoded in the point fill.

including 12 ASVs identified as Proteobacteria (including two Alphaproteobacteria ASVs and one Gammaproteobacteria ASV, genus *Aeromonas*), and one ASV was identified as an unassigned member of the phylum Firmicutes (Figure 3b). The ASV that was the most differentially abundant (from median abundance difference) in cyanobacterial tufts was a class-unresolved Proteobacteria, with a median abundance difference of −6.72 and an effect size of −0.87. In contrast, only six ASVs were significantly more abundant in turf algal samples, including five ASVs identified as Proteobacteria (including one Alphaproteobacteria ASV and one Gammaproteobacteria ASV, genus *Aeromonas*). The most differentially abundant ASV in turf algae was an unassigned species of the phylum Firmicutes, with a median abundance difference of 5.86 and an effect size of 0.73.

Next, metabarcoding data were subset to only include those ASVs assigned to the phylum Cyanobacteria ($n = 281$ unique ASVs) to compare the better the cyanobacterial assemblages between functional groups. Assessment of the phylogenetic relationships among these recovered cyanobacterial ASVs revealed extensive sample-specific diversification, with many ASVs displaying restricted distribution across samples and across sampled functional groups (Figure 4). However, 24.8% of cyanobacterial ASVs were found in at least one sample from both functional groups. One of the cyanobacterial ASVs was found in all samples. This shared cyanobacterial ASV was the single most abundant cyanobacterial ASV in four out of seven cyanobacterial tuft samples (57.1%) and five out of eight turf algal samples (62.5%; Figure 4, Appendix S1: Figure S6). Alpha diversity metrics were then calculated as done on the full ASV dataset from this cyanobacterial subset for both sampled benthic functional groups. The cyanobacterial subset assemblage did not vary significantly between cyanobacterial tufts and turf algae in richness (Chao1; PWRST, $p = 0.32$), diversity (Shannon-Weiner; PWRST, $p = 0.23$), or evenness (Pielou's Index; PWRST, $p = 0.34$; Appendix S1: Figure S7a). Principle coordinate analysis ordination based on a weighted UniFrac dissimilarity matrix calculated from this ASV-resolved cyanobacterial subset revealed no apparent clustering in cyanobacterial phylogenetic composition by functional group (Figure S7b; Axis 1 + 2 explained 50.3% of the total variation in cyanobacterial assemblage structure), further suggesting an overall congruence in the prokaryotic structure and phylogenetic relatedness of cyanobacterial tufts and turf algae when considering only the cyanobacterial assemblage.

Interestingly, the in situ yield was not significantly correlated with the underlying diversity (LM; all $p >> 0.5$) or structure (envfit; NMDS1 = −0.48, NMDS2 = 0.88, $r^2 = 0.27$, $p = 0.28$) of the whole prokaryotic assemblage or when considering only the diversity of cyanobacterial ASVs (LM; all $p >> 0.5$). The prokaryotic assemblage structure of those samples associated with the direction of the calculated higher yield vector (though notably not statistically significant) is graphically compared with those that were not associated with the direction of the yield vector in Appendix S1: Figure S8 to understand potential compositional determinants of increased yield better.

Both read-based and assembly-based metagenomic approaches demonstrate that cyanobacterial tufts are co-dominated by members of the bacterial Phyla Cyanobacteria and Proteobacteria

Abundance estimations were qualitatively similar between the two read-based estimators applied in this study. Both suggested a dominance of Cyanobacteria (Kaiju: 41.13% mean relative abundance; Metaphlan4: 24.65% mean relative abundance), primarily of the family Oscillatoriaceae (Kaiju: 33.25% mean relative abundance) comprised of the species *Okeania* sp *KiyG1* (Metaphlan4: 7.83% mean relative abundance) and *Okeania hirsuta* (Metaphlan4: 1.53% mean relative abundance; Figure 5). These cyanobacterial tufts were co-dominated by Proteobacteria (Kaiju: 38.36% mean relative abundance; Metaphlan4: 74.19% mean relative abundance). This compositional co-dominance was followed by members of the phylum Bacteroidota (Kaiju: 10.28% mean relative abundance; Metaphlan4: 0.91% mean relative abundance) and the phylum Planctomycetota (Kaiju: 3.07% mean relative abundance; Metaphlan4: 0.19% mean relative abundance; Figure 5). Abundance estimations diverged strongly between the two methods when estimating the abundance of different Proteobacterial taxa. Estimates from Kaiju suggested that these cyanobacterial tufts were dominated by members of the Alphaproteobacteria, particularly members of the important bacterial family involved in aquatic biofilm formation, Rhodobacteraceae (12.02% mean relative abundance; Elifantz et al., 2013), and Deltaproteobacteria, namely Desulfovibrionaceae (7.53% mean relative abundance; Figure 5b). Estimates from Metaphlan4 instead suggested a dominance of Gammaproteobacteria (69.95% mean relative abundance), driven primarily by the abundance of *Pseudomonas aeruginosa* (68.77% mean relative abundance; Figure 5a). Estimates from Metaphlan4 suggest that alphaproteobacterial abundance in cyanobacterial tufts is driven primarily by the marine bacterium *Ruegeria conchae* (1.53% mean relative abundance).

In addition to these alignment-based approaches on the quality-controlled paired-end reads, an assembly-based approach was applied to these shotgun metagenomic data to resolve the genomic identity of dominant cyanobacterial tuft community

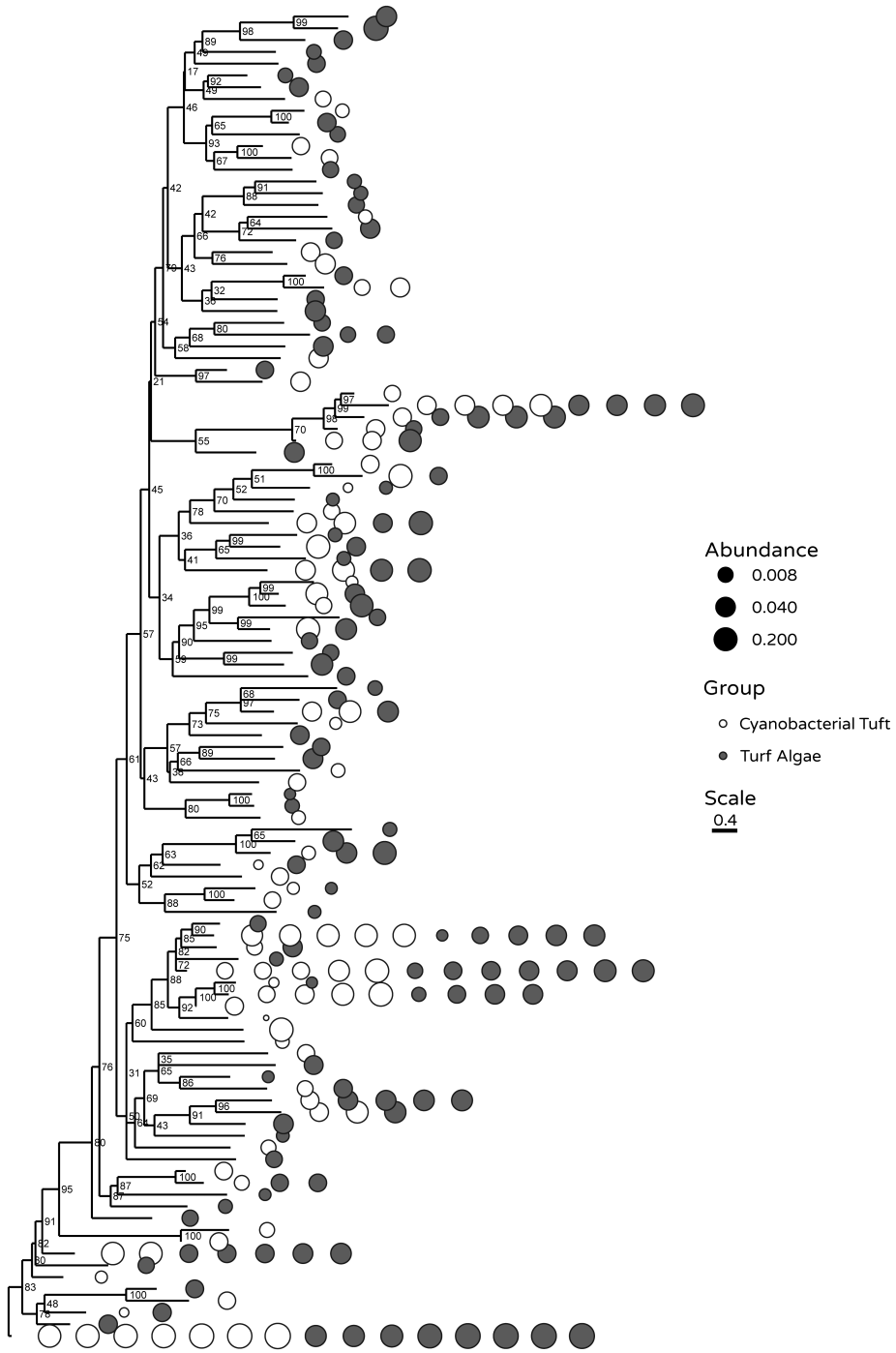

FIGURE 4 Dominant cyanobacterial ASVs are conserved between sampled benthic groups. Phylogenetic tree of recovered cyanobacterial amplicons. Circles denote per sample membership filled by functional group and sized by relative abundance. Node bootstrap support values are numerically given at each corresponding node. The scale bar encodes the raw cophenetic distance derived from the original hierarchical clustering of the distance matrix and does not approximate substitutions per site.

members through the recovery of MAGs and to increase the taxonomic resolution and confidence of taxonomic assignments. A total of 103 medium-to-high-quality MAGs were recovered and curated from these sequencing data. An overview of the general MAG stats (*CHECKM* completion and contamination), predicted taxonomy (GTDB), and relative abundance for each MAG in each sample are provided in Appendix S1: Table S5. Focusing on the level of individual MAG, a different cyanobacterial MAG within each metagenomic sample emerged as the most dominant component of each sample (Sample SC2: MAG ID = SC2_VAMB_17726, Length = 10.8 Mbp, Completion = 98.4%, Contamination = 2.26%, SC2 Relative Abundance = 18.6%, SC3 Relative Abundance = 2.4%; Sample SC3: MAG ID = SC3_metabat.36, Length = 9.0 Mbp, Completion = 97.74%, Contamination = 0.62%%, SC2 Relative

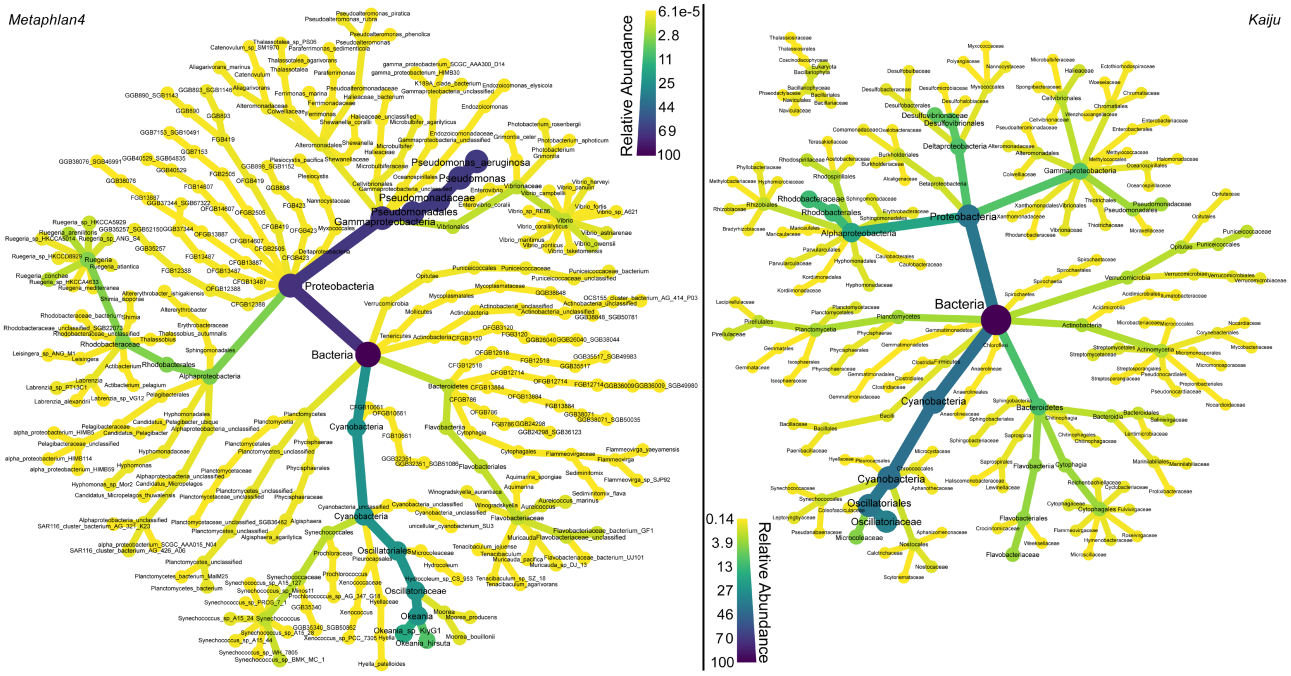

FIGURE 5 Read-based analyses suggest cyanobacterial tufts are co-dominated by Cyanobacteria and Proteobacteria. Left: Species-resolved hierarchy tree of cyanobacterial tuft community structure derived from Metaphlan4. Right: Family-resolved hierarchy tree of cyanobacterial tuft community structure derived from Kaiju. In both panels, the node and edge color and size are proportional to each node's mean relative abundance between shotgun metagenomic samples. Relative abundances are from total sum scaling normalized count data from read-level alignments. [Color figure can be viewed at wileyonlinelibrary.com]

Abundance = 0.59%, SC3 Relative Abundance = 55.1%) alongside a single subdominant cyanobacterial MAG present in only one sample (MAG ID = SC3_metabat.1_sub, Length = 3.9 Mbp, Completion = 75.37%, Contamination = 8.08%%, SC2 Relative Abundance = 0%, SC3 Relative Abundance = 0.56%), for a total of three cyanobacterial MAGs recovered from these sampled cyanobacterial tufts. Both dominant MAGs were annotated by *GTDB-tk* as belonging to unknown species within the cyanobacterial genus *Okeania* (Oscillatoriaceae) and were predicted to be closely related taxa (separated by a cophenetic distance of 0.023 on the calculated phylogenomic tree, Figure 6a; total Average Nucleotide Identity of 92.1 window size 500 bp). The subdominant cyanobacterial MAG was predicted to have been recovered from an unknown species within the toxin-producing cyanobacterial genus *Limnothrix* (Pseudanabaenaceae). These general taxonomic predictions on these dominant *Okeania* MAGs were congruent with those from both implemented read-based approaches (Figure 5). Read-based taxonomy alongside these phylogenomic and identity-based distance metrics suggested that these dominant *Okeania* MAGs were putatively similar strains of the species *Okeania hirsuta* or *Okeania* sp_*KiyG1* (species assignments from single-copy marker gene detection, Figure 5a), though, notably, cyanobacterial taxonomy ultimately requires a polyphasic approach to resolve species- and especially strain-level identity well (Komárek, 2016). Therefore, we treated these species-level assignments as putative and conservatively assigned both dominant cyanobacterial MAGs as different strains of a shared unknown species very likely belonging to the genus *Okeania*.

Still focusing on the level of individual MAG, both samples were compositionally co-dominated in abundance by a member of the Gammaproteobacteria annotated as belonging to the species *Pseudomonas aeruginosa* (SC2 Relative Abundance = 6.18%, SC3 Relative Abundance = 12.5%; Figure 6a). One of the sampled cyanobacterial tufts (sample SC2) also had an abundant MAG belonging to the Desulfovibrionaceae (SC2 Relative Abundance = 8.03%, SC3 Relative Abundance = 0%) that was uniquely observed in that tuft and an abundant member of the Opituales observed at low abundance in the other sample (SC2 Relative Abundance = 6.18%, SC3 Relative Abundance = 0.29%). The other sampled cyanobacterial tuft had two abundant members of the Cyclobacteriaceae in the Cytophagales that were both unique to that sample (MAG ID = SC3_metabat.14, SC2 Relative Abundance = 0%, SC3 Relative Abundance = 6.18%; MAG ID = SC2_metabat.6, SC2 Relative Abundance = 0%, SC3 Relative Abundance = 2.88%).

Aggregating MAG abundances at broader taxonomic scales, Cyanobacteria and Proteobacteria were predicted to co-dominate the cyanobacterial tufts, with mean relative abundances between the two shotgun metagenomic samples at 38.7% and

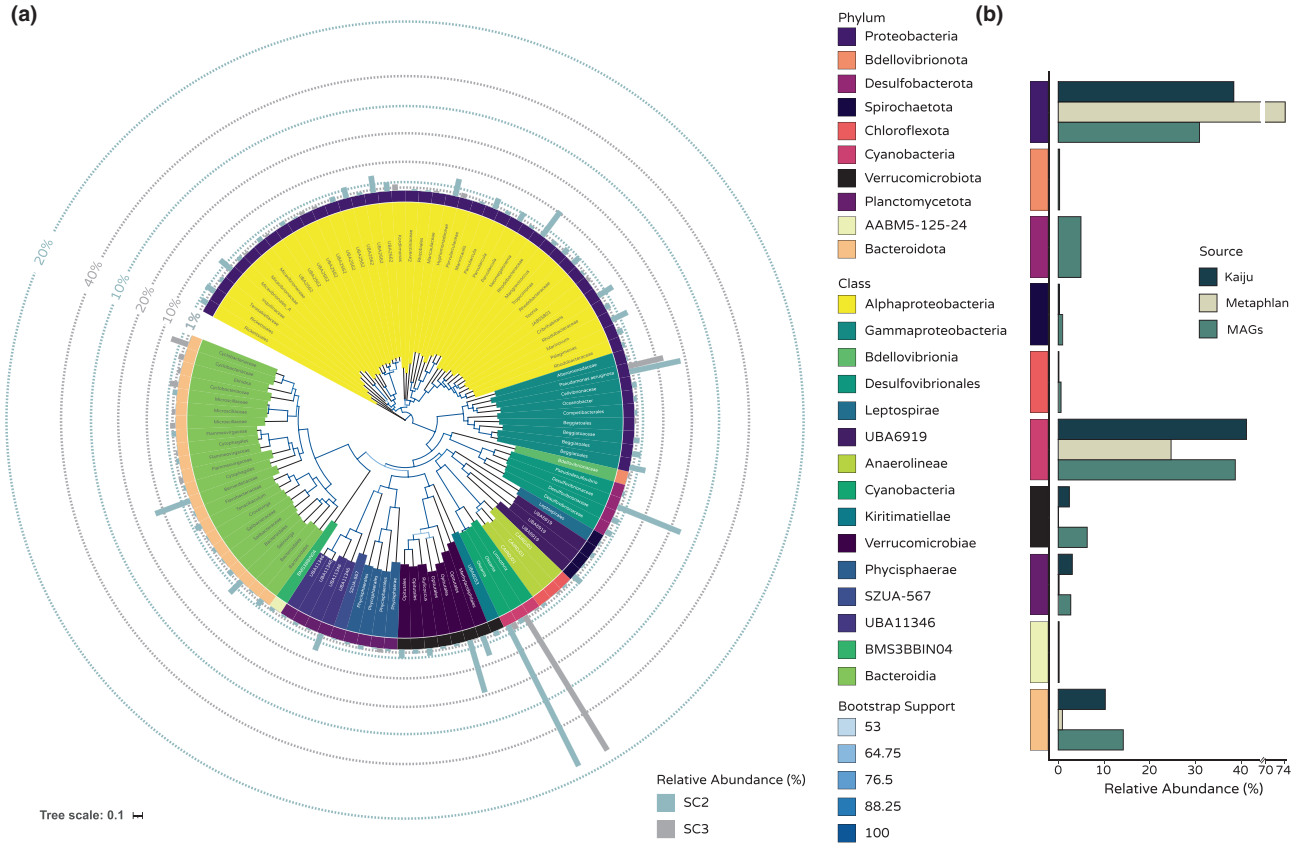

FIGURE 6 Florida Keys cyanobacterial tufts are built by closely related members of the cyanobacterial genus *Okeania*. (a) Phylogenomic tree of MAGs recovered from tufting cyanobacterial communities. The surrounding bar chart gives individual relative abundances within each metagenomic sample (note the different scales). Leaf nodes are colored by taxonomic class, with a corresponding color strip inclusively coloring by taxonomic phylum. Branches are colored by node bootstrap support value. Leaf labels give the lowest assigned taxonomic identity. (b) Bar plot of relative abundances of the recovered cyanobacterial tuft community aggregated at the level of taxonomic phyla. Colored bars on the *y*-axis follow the Phylum key in between panels. Individual bars are split and colored by the different abundance estimation methods (Kaiju, Metaphlan4, or MAG-based). [Color figure can be viewed at wileyonlinelibrary.com]

30.9% for Cyanobacteria and Proteobacteria, respectively (Figure 6b). Members of the Bacteroidota followed this co-dominance by these two phyla at a mean collective relative MAG abundance of 14.2% between the two samples. Phylum-level abundances were generally comparable across the three methods employed for estimating community composition in this study, with higher concordance between abundance estimates derived from Kaiju and MAG-based abundances than those derived from Metaphlan4 (Figure 6b). Few phyla were exclusively recovered using an assembly-based approach—notably including members of the Desulfobacterota, present at a mean collective MAG-based relative abundance of 4.96% across both samples. This highlights the utility of combining multiple computational approaches when resolving the community composition of complex environmental sequencing datasets. Members of the taxonomic class Alphaproteobacteria were numerically (by absolute MAG count) the most abundant members recovered from this assembly-based approach, with a total of 39 unique Alphaproteobacteria MAGs recovered collectively comprising 28.97% and 8.46% of the relative abundance space in samples SC2 and SC3, respectively (Figure 6a). Metagenome-assembled genomes belonging to the taxonomic class Bacteroidia were numerically co-dominant, with a total of 22 unique Bacteroidia MAGs recovered collectively comprising 11.23% and 17.2% of the total MAG-based composition in samples SC2 and SC3, respectively. Members of the taxonomic class Gammaproteobacteria, though numerically less dominant than their Alphaproteobacterial relatives (a total of nine unique MAGs curated), comprised 11.24% and 13.06% of the total MAG-based composition in samples SC2 and SC3, respectively. This high abundance was driven primarily by the abundance of a single MAG annotated as belonging to *Pseudomonas aeruginosa*, consistent with abundance estimates from Metaphlan4 (Figures 5a and 6a).

DISCUSSION

Here, we document the in situ photophysiology and prokaryotic assemblage structure of epilithic tufting

cyanobacterial communities and turf algal communities on a reef site in the Florida Keys Reef Tract. Overall, we reveal a general convergence in the photophysiology and prokaryotic assemblage structure between these important algal groups. Though the mean photosynthetic yield did not differ between cyanobacterial tufts and turf algal communities, the associated variability in yield did (Figure 1). The net primary production of benthic substrates dominated by cyanobacterial mats has also recently been reported to have a higher associated variance than the carbon flux associated with algal turf-dominated substrates (Webb et al., 2021). When paired with our results (Figure 1), this suggests that an increase in spatial variability in basal carbon cycling could accompany the expanding cover of benthic cyanobacterial aggregations on reefs. This will hold especially true if cyanobacterial expansion comes at the expense of algal turf cover or exacerbates the prokaryotic (particularly cyanobacterial) taxonomic homogenization between conspicuous benthic cyanobacterial aggregations and turf algae similar to that documented in this study (Figures 2–4). Increasing taxonomic homogenization in the cyanobacterial assemblage between complex cyanobacterial assemblages and algal turfs may increase DOC release on future reefs and accelerate the process of reef microbialization (Haas et al., 2016; Mueller et al., 2022). Further work should seek to disentangle competitive dynamics between benthic cyanobacterial aggregations and algal turfs, similar to work on the competitive dynamics between benthic cyanobacterial mats and macroalgae (Tack, 2019; Thacker & Paul, 2001) to better contextualize and project these assessments of photophysiology to the spatial and functional ecology of future reef carbon cycling.

Our findings of minimal differences in the prokaryotic assemblage structure (Figures 2 and 3)—including few differences within the cyanobacterial assemblage (Figure 4)—between turf algal communities and benthic cyanobacterial tufts have important implications for consumer-resource dynamics on future reefs. In particular, this overall congruence brings additional attention to the longstanding paradigm that mobile consumers typically preferentially target algal turfs while avoiding complex cyanobacterial-dominated assemblages such as benthic cyanobacterial mats. The presence of similar cyanobacterial assemblages in frequently targeted turf algae communities (Adam et al., 2018; Bruggemann et al., 1994) questions this generality. Cyanobacterial avoidance by consumers has long been associated with the production of toxins by the mat-building cyanobacteria, though notably, this evidence stems primarily from work on the polyphyletic genus *Lyngbya* (Capper et al., 2006; Capper & Paul, 2008; Thacker et al., 1997). Only a single biosynthetic gene cluster with similarity to a known toxin-producing gene cluster (malyngamide I) was identified in the dominant cyanobacterial MAGs recovered from the sequenced tufts (Appendix S1: Table S6). Emerging evidence from examination of the nutritional ecology of nominal herbivores, specifically reef parrotfishes, suggests a fundamental preference for targeting cyanobacteria as nutritional resources by these fishes (Clements et al., 2017; Nicholson & Clements, 2020, 2023). Alongside this evidence from nutritional ecology, multiple observational studies now have confirmed the consumption of benthic cyanobacterial mats by multiple nominally herbivorous fishes on Caribbean reefs (Cissell et al., 2019; Cissell & McCoy, 2022b), including the documented preferential consumption by several of these fishes (Manning & McCoy, 2023). These various lines of evidence imply that the expansion of conspicuous benthic cyanobacterial assemblages may not inherently disrupt trophic flow through ecosystems (here, on coral reefs) owing to a lack of palatability as previously generally theorized (Ullah et al., 2018). The consistently short thallus length of turfs at this site (<1.0 cm) suggests a robust site-scale grazing pressure (Connell et al., 2014), potentially extending to these epilithic cyanobacterial communities. Indeed, reefs on the Florida Keys reef tract are marked by a relatively healthy fish assemblage that can heavily graze the reef substrate (Lester et al., 2020). However, conflicting observational work leaves the overall generalizability of the targeting of benthic cyanobacterial aggregations equivocal (de Ribeiro et al., 2022; Ford et al., 2021), with potential geographic differences driven by fish assemblage structure, cyanobacterial identity, relative toxin production, and physical growth habit (Cissell & McCoy, 2022a). Further work should specifically monitor grazing pressure on benthic cyanobacterial assemblages at this site, both to better understand if this strong grazing pressure contributes to the relatively low benthic coverage of conspicuous cyanobacterial assemblages at this site (Figure S1) and to contribute to this bourgeoning literature on geographic patterns in predation pressure on benthic cyanobacterial communities.

The ubiquitous distribution of the dominant recovered cyanobacterial ASV and the shared distribution patterns of many subdominant cyanobacterial ASVs across functional groups suggest a potential role of algal turfs as reservoirs of tuft- and mat-forming cyanobacterial taxa on coral reefs (Figure 4, Figures S6 and S7). Brocke et al. (2018) recently documented a similar congruence in the identity of dominant cyanobacterial members between benthic cyanobacterial mats and algal turfs sampled in Curaçao, where the identified cyanobacterial taxa from modern microbial mats had also been observed in algal turfs previously sampled in 1975 (van den Hoek et al., 1975). Further, previous microscopy-based analyses of algal turf succession patterns suggest the presence of cyanobacterial taxa that are closely related to known mat-forming cyanobacteria in algal turfs (Cissell & McCoy, 2022b;

Fricke et al., 2011). We note, however, that while the diversity and identity of dominant Cyanobacteria in each of these turfs are similar, the overall biomass of Cyanobacteria is likely to be lower in algal turf substrates. Regardless, the dynamics and timing of this apparent cyanobacterial homogenization (Figure 4) present open and interesting lines of inquiry, motivating specifically the following questions: (1) Do dominant tufting cyanobacteria intrude into existing turf communities from the expansion of benthic cover of cyanobacterial tufts? (2) Are dominant tufting cyanobacteria recruited into early successional algal turf communities where these turfs represent an alternate successional state for these benthic cyanobacteria? (3) Are these dominant tufting cyanobacteria able to be viably released from these turfs (e.g., from mechanical dislodging from grazing pressure) to subsequently establish new cyanobacterial tufts (i.e., algal turfs as net benthic cyanobacterial tuft reservoirs) or do turfs represent successional "dead ends" for these benthic cyanobacteria (i.e., algal turfs as net benthic cyanobacterial tuft sinks)? Polyphasic approaches that incorporate genome-resolved data (ideally from isolates) from samples taken of both tufting cyanobacterial communities and turf algal communities at different successional states would be helpful to (1) offer further support that the dominant cyanobacterial genome is shared between functional groups and (2) address many of these above posited lines of inquiry. Further, more work should be directed toward resolving abundance-based differences in cyanobacterial members between these groups, which may be substantial.

The community composition aggregated at broad taxonomic levels was similar between the different sequencing methods utilized herein and was similar to previous shotgun metagenomic and metabarcoding assessments of cyanobacterial mat community structure (Figures 5 and 6, Figure S5; Biessy et al., 2021; Cissell & McCoy, 2021; Cleary et al., 2019; Stuij et al., 2022). Members of the genus *Okeania* have previously been observed to dominate benthic cyanobacterial mats and cyanobacterial tufts, including tufts of similar color and growth habit (Engene et al., 2013). *Pseudomonas aeruginosa*, another dominant member of the sampled cyanobacterial tufts, is a ubiquitous environmental bacterium that is generally associated with biofilm formation (Haussler, 2004) but has not been generally described in association with marine cyanobacterial tuft assemblages. A recent comparison of mat community structure across different underlying substrate types revealed no significant effects of underlying growth substrate type on community structure, including between epipelic, horizontally spreading mat carpets and epilithic, tufting cyanobacterial communities similar to those sampled in this study (Stuij et al., 2022). These authors also found significant variability within the cyanobacterial-associated prokaryotic assemblage among their sampled cyanobacterial mats. Both findings align with those presented here (Figures 3a, 5 and 6). Our results suggest a great degree of similarity at a coarse taxonomic resolution between benthic cyanobacterial mats and the epilithic cyanobacterial mats, with tuft-specific (spatial) diversification and heterogeneity both at the ASV level (Figure 3a) and within the genomic identity of dominant community members (Figure 6a). This suggests that a distinction between benthic cyanobacterial mats and benthic cyanobacterial tufts may indeed be nominal. However, further work is still needed to confirm the utility or futility of their semantic distinction. Our metabarcoding-based assessment of the prokaryotic assemblage structure of turf algae was also congruent with previous sequencing-based assessments of turf microbial community structure, especially in its suggestion of the overall importance of members of the Alphaproteobacteria (Figure S5; Hester et al., 2016).

Our results motivate increased attention toward comparing the ecology of these dominant benthic functional groups. Indeed, the primary differentiating compositional features among algal turfs and tufting cyanobacterial communities may primarily reside in the eukaryotic microalgal assemblage, which was not interrogated in this study, leaving many open questions and opportunities for research. The apparent convergence in both the photophysiology and prokaryotic assemblage structure (particularly in the cyanobacterial assemblage) between proliferating conspicuous benthic cyanobacterial aggregations and ubiquitous turf algae have serious ecophysiological implications for future reefs, especially in the calculation of future reef carbon stoichiometry and overall carbon budgets.

It should be noted, however, that these cyanobacterial tufts were present at low benthic coverage at a level that would be expected in a "healthy" reef environment (Figure S1). This may imply that these tufts are different from the benthic cyanobacterial assemblages that can become dominant or form extensive blooms on reefs. Bloom-forming benthic cyanobacteria may have distinct composition and functional ecology from those studied here. Our results may also impact the importance of distinguishing between cyanobacterial tufts and turf algae during the application of semi-automatic photo annotation. The importance of distinguishing between them depends greatly on the goal of the photo classification, for example, providing justification to group these substrates when used to inform the calculation of reef carbon budgets while remaining an important distinction for monitoring trajectories of benthic reef change. We urge further research that builds upon the results of this study from diverse geographic locales to capture spatial and temporal variability in this apparent taxonomic and functional homogenization.

AUTHOR CONTRIBUTIONS

Ethan C. Cissell: Conceptualization (equal); data curation (lead); formal analysis (lead); investigation (lead); methodology (lead); software (lead); visualization (lead); writing – original draft (lead); writing – review and editing (supporting). **Sophie J. McCoy:** Conceptualization (equal); funding acquisition (lead); investigation (supporting); resources (lead); supervision (lead); validation (lead); writing – review and editing (lead).

ACKNOWLEDGMENTS

This work was supported by grants from the Florida "Protect Our Reefs" Grants Program (POR_2020_03) and the Tatelbaum Ocean Research Fund awarded to S. McCoy. E. Cissell was supported by a National Science Foundation Graduate Research Fellowship (Grant Number: 074012-520-044116). We extend our thanks to J. Delaney and A. Bruckner for research permissions to conduct this work in the Florida Keys National Marine Sanctuary. We are grateful for the assistance of D. Barnes and C. Morris for assistance in the field. We thank C. Peters and the Florida State University Coastal and Marine Laboratory for diving and marine vessel support. We thank A. Brown and the Florida State University Department of Biological Science Core Facility for discussions and assistance during DNA extraction and library preparation and S. Kranz for the provision of nutrient data. Finally, we thank J. Manning for the discussions and feedback on earlier versions of this manuscript.

ORCID

Ethan C. Cissell https://orcid.org/0000-0003-2756-0262
Sophie J. McCoy https://orcid.org/0000-0003-1324-1578

REFERENCES

Abdala Asbun, A., Besseling, M. A., Balzano, S., van Bleijswijk, J. D. L., Witte, H. J., Villanueva, L., & Engelmann, J. C. (2020). Cascabel: A scalable and versatile amplicon sequence data analysis pipeline delivering reproducible and documented results. *Frontiers in Genetics*, *11*, 489357.

Adam, T., Duran, A., Fuchs, C., Roycroft, M., Rojas, M., Ruttenberg, B., & Burkepile, D. (2018). Comparative analysis of foraging behavior and bite mechanics reveals complex functional diversity among Caribbean parrotfishes. *Marine Ecology Progress Series*, *597*, 207–220.

Albert, S., O'Neil, J. M., Udy, J. W., Ahern, K. S., O'Sullivan, C. M., & Dennison, W. C. (2005). Blooms of the cyanobacterium *Lyngbya majuscula* in coastal Queensland, Australia: Disparate sites, common factors. *Marine Pollution Bulletin*, *51*, 428–437.

Arp, G., Reimer, A., & Reitner, J. (1999). Calcification in cyanobacterial biofilms of alkaline salt lakes. *European Journal of Phycology*, *34*, 393–403.

Barott, K. L., Rodriguez-Brito, B., Janouškovec, J., Marhaver, K. L., Smith, J. E., Keeling, P., & Rohwer, F. L. (2011). Microbial diversity associated with four functional groups of benthic reef algae and the reef-building coral *Montastraea annularis*: Microbial diversity on benthic algae and corals. *Environmental Microbiology*, *13*, 1192–1204.

Biessy, L., Wood, S. A., Chinain, M., Roué, M., & Smith, K. F. (2021). Exploring benthic cyanobacterial diversity and co-occurring potentially harmful dinoflagellates in six islands of the South Pacific. *Hydrobiologia*, *848*, 2815–2829.

Blanco-Miguez, A., Beghini, F., Cumbo, F., McIver, L. J., Thompson, K. N., Zolfo, M., Manghi, P., Dubois, L., Huang, K. D., Thomas, A., Piccinno, G., Piperni, E., Punčochář, M., MireiaValles-Colomer, A. T., Giordano, F., Davies, R., Wolf, J., Berry, S. E., Spector, T. D., … Segata, N. (2023). Extending and improving metagenomic taxonomic profiling with uncharacterized species with MetaPhlAn 4. *Nature Biotechnology*, *41*, 1633–1644. https://doi.org/10.1038/s41587-023-01688-w

Blin, K., Shaw, S., Kloosterman, A. M., Charlop-Powers, Z., van Wezel, G. P., Medema, M. H., & Weber, T. (2021). antiSMASH 6.0: Improving cluster detection and comparison capabilities. *Nucleic Acids Research*, *49*, W29–W35.

Bowers, R. M., Kyrpides, N. C., Kyrpides, N. C., Harmon-Smith, M., Doud, D., Reddy, T. B. K., Schulz, F., Jarett, J., Rivers, A. R., Eloe-Fadrosh, E. A., Tringe, S. G., Ivanova, N. N., Copeland, A., Clum, A., Becraft, E. D., Malmstrom, R. R., Birren, B., Podar, M., Bork, P., … Woyke, T. (2017). Minimum information about a single amplified genome (MISAG) and a metagenome-assembled genome (MIMAG) of bacteria and archaea. *Nature Biotechnology*, *35*, 725–731.

Brocke, H. J., Piltz, B., Herz, N., Abed, R. M. M., Palinska, K. A., John, U., dan Haan, J., de Beer, D., & Nugues, M. M. (2018). Nitrogen fixation and diversity of benthic cyanobacterial mats on coral reefs in Curaçao. *Coral Reefs*, *37*, 861–874.

Brocke, H. J., Wenzhoefer, F., de Beer, D., Mueller, B., van Duyl, F. C., & Nugues, M. M. (2015). High dissolved organic carbon release by benthic cyanobacterial mats in a Caribbean reef ecosystem. *Scientific Reports*, *5*, 8852.

Bruggemann, J. H., Kuyper, M. W. M., & Breeman, A. M. (1994). Comparative analysis of foraging and habitat use by the sympatric Caribbean parrotfish Scarus vetula and Sparisoma viride (Scaridae). *Marine Ecology Progress Series*, *112*, 51–66.

Callahan, B. J., McMurdie, P. J., Rosen, M. J., Han, A. W., Johnson, A. J. A., & Holmes, S. P. (2016). DADA2: High-resolution sample inference from Illumina amplicon data. *Nature Methods*, *13*, 581–583.

Capper, A., Cruz-Rivera, E., Paul, V. J., & Tibbetts, I. R. (2006). Chemical deterrence of a marine *Cyanobacterium* against sympatric and non-sympatric consumers. *Hydrobiologia*, *553*, 319–326.

Capper, A., & Paul, V. J. (2008). Grazer interactions with four species of Lyngbya in Southeast Florida. *Harmful Algae*, *7*, 717–728.

Chaumeil, P.-A., Mussig, A. J., Hugenholtz, P., & Parks, D. H. (2019). GTDB-Tk: A toolkit to classify genomes with the genome taxonomy database. *Bioinformatics*, *36*, 1925–1927.

Cissell, E. C., Eckrich, C. E., & McCoy, S. J. (2022). Cyanobacterial mats as benthic reservoirs and vectors for coral black band disease pathogens. *Ecological Applications*, *32*, e2692.

Cissell, E. C., Manning, J. C., & McCoy, S. J. (2019). Consumption of benthic cyanobacterial mats on a Caribbean coral reef. *Scientific Reports*, *9*, 12693.

Cissell, E. C., & McCoy, S. J. (2021). Shotgun metagenomic sequencing reveals the full taxonomic, trophic, and functional diversity of a coral reef benthic cyanobacterial mat from Bonaire, Caribbean Netherlands. *Science of the Total Environment*, *755*, 142719.

Cissell, E. C., & McCoy, S. J. (2022a). Marine cyanobacteria in the Anthropocene: Are top-down paradigms robust to climate change? *Climate Change Ecology*, *3*, 100057.

Cissell, E. C., & McCoy, S. J. (2022b). *Predation, community asynchrony, and metacommunity stability in cyanobacterial mats*. bioRxiv. https://doi.org/10.1101/2022.10.07.511315

Cissell, E. C., & McCoy, S. J. (2023a). Top-heavy trophic structure within benthic viral dark matter. *Environmental Microbiology*, *25*, 2303–2320.

Cissell, E. C., & McCoy, S. J. (2023b). Viral association with cyanobacterial mat community mortality. *Ecology*, *104*, e4131.

Cleary, D. F. R., Polónia, A. R. M., Huang, Y. M., Putchakarn, S., Gomes, N. C. M., & de Voogd, N. J. (2019). A comparison of prokaryote communities inhabiting sponges, bacterial mats, sediment and seawater in southeast Asian coral reefs. *FEMS Microbiology Ecology*, *95*, fiz169.

Clements, K. D., German, D., Piché, J., Tribollet, A., & Choat, J. H. (2017). Integrating ecological roles and trophic diversification on coral reefs: Multiple lines of evidence identify parrotfishes as microphages. *Biological Journal of the Linnean Society*, *120*, 729–751.

Connell, S., Foster, M., & Airoldi, L. (2014). What are algal turfs? Towards a better description of turfs. *Marine Ecology Progress Series*, *495*, 299–307.

Dacey, D. P., & Chain, F. J. J. (2021). Concatenation of paired-end reads improves taxonomic classification of amplicons for profiling microbial communities. *BMC Bioinformatics*, *22*, 493.

de Bakker, D. M., van Duyl, F. C., Bak, R. P. M., Nugues, M. M., Nieuwland, G., & Meesters, E. H. (2017). 40 years of benthic community change on the Caribbean reefs of Curaçao and Bonaire: The rise of slimy cyanobacterial mats. *Coral Reefs*, *36*, 355–367.

de Ribeiro, F. V., Cairesia, T. A., de Simões, M. A. A., Hargreaves, P. I., Villela, L. B., de Fistarol, G. O., Caselgrandi, A. B., Cazelgrandi Junior, A. B., de Moura, R. L., Pereira, R. C., Pereira-Filho, G. H., & Salomon, P. S. (2022). Benthic cyanobacterial diversity and antagonistic interactions in Abrolhos Bank: Allelopathy, susceptibility to herbivory, and toxicity. *Frontiers in Marine Science*, *8*, 790277.

den Haan, J., Huisman, J., Brocke, H. J., Goehlich, H., Latijnhouwers, K. R. W., van Heeringen, S., Honcoop, S. A. S., Bleyenberg, T. E., Schouten, S., Cerli, C., Hoitinga, L., Vermeij, M. J. A., & Visser, P. M. (2016). Nitrogen and phosphorus uptake rates of different species from a coral reef community after a nutrient pulse. *Scientific Reports*, *6*, 28821.

Echenique-Subiabre, I., Villeneuve, A., Golubic, S., Turquet, J., Humbert, J.-F., & Gugger, M. (2015). Influence of local and global environmental parameters on the composition of cyanobacterial mats in a tropical lagoon. *Microbial Ecology*, *69*, 234–244.

Elifantz, H., Horn, G., Ayon, M., Cohen, Y., & Minz, D. (2013). Rhodobacteraceae are the key members of the microbial community of the initial biofilm formed in eastern Mediterranean coastal seawater. *FEMS Microbiology Ecology*, *85*, 348–357.

Engene, N., Paul, V. J., Byrum, T., Gerwick, W. H., Thor, A., & Ellisman, M. H. (2013). Five chemically rich species of tropical marine cyanobacteria of the genus *Okeania* gen. Nov. (Oscillatoriales, Cyanoprokaryota). *Journal of Phycology*, *49*, 1095–1106.

Feltz, C. J., & Miller, G. E. (1996). An aymptotic test for the equality of coefficients of variation from k populations. *Statistics in Medicine*, *15*, 647–658.

Fernandes, A. D., Macklaim, J. M., Linn, T. G., Reid, G., & Gloor, G. B. (2013). ANOVA-Like Differential Expression (ALDEx) analysis for mixed population RNA-Seq. *PLoS ONE*, *8*, e67019.

Ford, A. K., Bejarano, S., Nugues, M. M., Visser, P. M., Albert, S., & Ferse, S. C. A. (2018). Reefs under siege—The rise, putative drivers, and consequences of benthic cyanobacterial Mats. *Frontiers in Marine Science*, *5*, 18.

Ford, A. K., van Hoytema, N., Moore, B. R., Pandihau, L., Wild, C., & Ferse, S. C. A. (2017). High sedimentary oxygen consumption indicates that sewage input from small islands drives benthic community shifts on overfished reefs. *Environmental Conservation*, *44*, 405–411.

Ford, A. K., Visser, P. M., van Herk, M. J., Jongepier, E., & Bonito, V. (2021). First insights into the impacts of benthic cyanobacterial mats on fish herbivory functions on a nearshore coral reef. *Scientific Reports*, *11*, 7147.

Fricke, A., Teichberg, M., Beilfuss, S., & Bischof, K. (2011). Succession patterns in algal turf vegetation on a Caribbean coral reef. *Botanica Marina*, *54*, 111–126.

García-Robledo, E., Corzo, A., & Papaspyrou, S. (2014). A fast and direct spectrophotometric method for the sequential determination of nitrate and nitrite at low concentrations in small volumes. *Marine Chemistry*, *162*, 30–36.

Goatley, C. H. R., Bonaldo, R. M., Fox, R. J., & Bellwood, D. R. (2016). Sediments and herbivory as sensitive indicators of coral reef degradation. *Ecology and Society*, *21*, 29.

Gurevich, A., Saveliev, V., Vyahhi, N., & Tesler, G. (2013). QUAST: Quality assessment tool for genome assemblies. *Bioinformatics*, *29*, 1072–1075.

Haas, A. F., Fairoz, M. F. M., Kelly, L. W., Nelson, C. E., Dinsdale, E. A., Edwards, R. A., Giles, S., Hatay, M., Hisakawa, N., Knowles, B., Lim, Y. W., Maughan, H., Pantos, O., Roach, T. N. F., Sanchez, S. E., Silveira, C. B., Sandin, S., Smith, J. E., & Rohwer, F. (2016). Global microbialization of coral reefs. *Nature Microbiology*, *1*, 16042.

Habibah, N., Sundari, H., & Hadi, M. C. (2018). A simple spectrophotometric method for the quantitative analysis of phosphate in the water samples. *Jurnal Sains dan Teknologi*, *7*, 198–204.

Haussler, S. (2004). Biofilm formation by the small colony variant phenotype of *Pseudomonas aeruginosa*. *Environmental Microbiology*, *6*, 546–551.

Herlemann, D. P. R., Geissinger, O., & Brune, A. (2007). The termite group I phylum is highly diverse and widespread in the environment. *Applied and Environmental Microbiology*, *73*, 6682–6685.

Hester, E. R., Barott, K. L., Nulton, J., Vermeij, M. J., & Rohwer, F. L. (2016). Stable and sporadic symbiotic communities of coral and algal holobionts. *The ISME Journal*, *10*, 1157–1169.

Jain, C., Rodriguez-R, L. M., Phillippy, A. M., Konstantinidis, K. T., & Aluru, S. (2018). High throughput ANI analysis of 90K prokaryotic genomes reveals clear species boundaries. *Nature Communications*, *9*, 5114.

Jouffray, J.-B., Nyström, M., Norström, A. V., Williams, I. D., Wedding, L. M., Kittinger, J. N., & Williams, G. J. (2015). Identifying multiple coral reef regimes and their drivers across the Hawaiian archipelago. *Philosophical Transactions of the Royal Society, B: Biological Sciences*, *370*, 20130268.

Kalyaanamoorthy, S., Minh, B. Q., Wong, T. K. F., von Haeseler, A., & Jermiin, L. S. (2017). ModelFinder: Fast model selection for accurate phylogenetic estimates. *Nature Methods*, *14*, 587–589.

Kang, D. D., Li, F., Kirton, E., Thomas, A., Egan, R., An, H., & Wang, Z. (2019). MetaBAT 2: An adaptive binning algorithm for robust and efficient genome reconstruction from metagenome assemblies. *PeerJ*, *7*, e7359.

Kang, J., Mohamed, H. F., Liu, X., Pei, L., Huang, S., Lin, X., Zheng, X., & Luo, Z. (2022). Combined culture and DNA metabarcoding analysis of cyanobacterial community structure in response to coral reef health status in the South China Sea. *Journal of Marine Science and Engineering*, *10*, 1984.

Katoh, K., & Standley, D. M. (2013). MAFFT multiple sequence alignment software version 7: Improvements in performance and usability. *Molecular Biology and Evolution*, *30*, 772–780.

Klindworth, A., Pruesse, E., Schweer, T., Peplies, J., Quast, C., Horn, M., & Glöckner, F. O. (2013). Evaluation of general 16S ribosomal RNA gene PCR primers for classical and next-generation sequencing-based diversity studies. *Nucleic Acids Research*, *41*, e1.

Klumpp, D. W., & McKinnon, A. D. (1989). Temporal and spatial patterns in primary production of a coral-reef epilithic algal

community. *Journal of Experimental Marine Biology and Ecology*, *131*, 1–22.
Komárek, J. (2016). A polyphasic approach for the taxonomy of cyanobacteria: Principles and applications. *European Journal of Phycology*, *51*, 346–353.
Krishnamoorthy, K., & Lee, M. (2014). Improved tests for the equality of normal coefficients of variation. *Computational Statistics*, *29*, 215–232.
Langmead, B., & Salzberg, S. L. (2012). Fast gapped-read alignment with bowtie 2. *Nature Methods*, *9*, 357–359.
Lester, S. E., Rassweiler, A., McCoy, S. J., Dubel, A. K., Donovan, M. K., Miller, M. W., Miller, S. D., Ruttenberg, B. I., Samhouri, J. F., & Hay, M. E. (2020). Caribbean reefs of the Anthropocene: Variance in ecosystem metrics indicates bright spots on coral depauperate reefs. *Global Change Biology*, *26*, 4785–4799.
Letunic, I., & Bork, P. (2021). Interactive tree of life (iTOL) v5: An online tool for phylogenetic tree display and annotation. *Nucleic Acids Research*, *49*, W293–W296.
Manning, J. C., & McCoy, S. J. (2023). Preferential consumption of benthic cyanobacterial mats by Caribbean parrotfishes. *Coral Reefs*, *42*, 967–975.
McMurdie, P. J., & Holmes, S. (2013). Phyloseq: An R package for reproducible interactive analysis and graphics of microbiome census data. *PLoS ONE*, *8*, e61217.
Menzel, P., Ng, K. L., & Krogh, A. (2016). Fast and sensitive taxonomic classification for metagenomics with Kaiju. *Nature Communications*, *7*, 11257.
Minh, B. Q., Schmidt, H. A., Chernomor, O., Schrempf, D., Woodhams, M. D., von Haeseler, A., & Lanfear, R. (2020). IQ-TREE 2: New models and efficient methods for phylogenetic inference in the genomic era. *Molecular Biology and Evolution*, *37*, 1530–1534.
Mueller, B., Brocke, H. J., Rohwer, F. L., Dittmar, T., Huisman, J., Vermeij, M. J. A., & de Goeij, J. M. (2022). Nocturnal dissolved organic matter release by turf algae and its role in the microbialization of reefs. *Functional Ecology*, *36*, 2104–2118.
Mueller, B., van der Zande, R., Van Leent, P., Meesters, E., Vermeij, M., & Van Duyl, F. (2014). Effect of light availability on dissolved organic carbon release by Caribbean reef algae and corals. *Bulletin of Marine Science*, *90*, 875–893.
Nicholson, G. M., & Clements, K. D. (2020). Resolving resource partitioning in parrotfishes (Scarini) using microhistology of feeding substrata. *Coral Reefs*, *39*, 1313–1327.
Nicholson, G. M., & Clements, K. D. (2023). Micro-photoautotroph predation as a driver for trophic niche specialization in 12 syntopic Indo-Pacific parrotfish species. *Biological Journal of the Linnean Society*, *139*, 91–114.
Nissen, J. N., Johansen, J., Allesøe, R. L., Sønderby, C. K., Armenteros, J. J. A., Grønbech, C. H., Jensen, L. J., Nielsen, H. B., Petersen, T. N., Winther, O., & Rasmussen, S. (2021). Improved metagenome binning and assembly using deep variational autoencoders. *Nature Biotechnology*, *39*, 555–560.
Odum, H. T., & Odum, E. P. (1955). Trophic structure and productivity of a windward coral reef community on Eniwetok atoll. *Ecological Monographs*, *25*, 291–320.
Olm, M. R., Brown, C. T., Brooks, B., & Banfield, J. F. (2017). dRep: A tool for fast and accurate genomic comparisons that enables improved genome recovery from metagenomes through dereplication. *The ISME Journal*, *11*, 2864–2868.
Parks, D. H., Imelfort, M., Skennerton, C. T., Hugenholtz, P., & Tyson, G. W. (2015). CheckM: Assessing the quality of microbial genomes recovered from isolates, single cells, and metagenomes. *Genome Research*, *25*, 1043–1055.
Paul, V. J., Thacker, R. W., Banks, K., & Golubic, S. (2005). Benthic cyanobacterial bloom impacts the reefs of South Florida (Broward County, USA). *Coral Reefs*, *24*, 693–697.
Peng, Y., Leung, H. C. M., Yiu, S. M., & Chin, F. Y. L. (2012). IDBA-UD: A de novo assembler for single-cell and metagenomic sequencing data with highly uneven depth. *Bioinformatics*, *28*, 1420–1428.
Puyana, M., Prato, J. A., Nieto, C. F., Ramos, F. A., Castellanos, L., Pinzón, P., & Zárate, J. C. (2019). Experimental approaches for the evaluation of allelopathic interactions between hermatypic corals and marine benthic Cyanobacteria in the Colombian Caribbean. *Acta Biológica Colombiana*, *24*, 243–254.
Quast, C., Pruesse, E., Yilmaz, P., Gerken, J., Schweer, T., Yarza, P., Peplies, J., & Glöckner, F. O. (2012). The SILVA ribosomal RNA gene database project: Improved data processing and web-based tools. *Nucleic Acids Research*, *41*, D590–D596.
Rodriguez-R, L. M., Gunturu, S., Tiedje, J. M., Cole, J. R., & Konstantinidis, K. T. (2018). Nonpareil 3: Fast estimation of metagenomic coverage and sequence diversity. *mSystems*., *3*, e00039-18. https://doi.org/10.1128/msystems.00039-18
Silva, L., Calleja, M. L., Ivetic, S., Huete-Stauffer, T., Roth, F., Carvalho, S., & Morán, X. A. G. (2021). Heterotrophic bacterioplankton responses in coral- and algae-dominated Red Sea reefs show they might benefit from future regime shift. *Science of the Total Environment*, *751*, 141628.
Smith, J. E., Brainard, R., Carter, A., Grillo, S., Edwards, C., Harris, J., Lewis, L., Obura, D., Rohwer, F., Sala, E., Vroom, P. S., & Sandin, S. (2016). Re-evaluating the health of coral reef communities: Baselines and evidence for human impacts across the Central Pacific. *Proceedings of the Royal Society B: Biological Sciences*, *283*, 20151985.
Stal, L. J. (1995). Tansley review No. 84 physiological ecology of cyanobacteria in microbial mats and other communities. *The New Phytologist*, *131*, 1–32.
Stuij, T. M., Cleary, D. F., Gomes, N., Mehrotra, R., Visser, P. M., Speksnijder, A. G., & Hoeksema, B. W. (2022). High diversity of benthic cyanobacterial mats on coral reefs of Koh Tao, Gulf of Thailand. *Coral Reefs*, *42*, 77–91.
Tack, L. F. J. (2019). *Dynamics of dictyota and benthic cyanobacterial Mats (BCMs) on the shallow coral reefs of Bonaire*. [Master's Thesis, University of Amsterdam]. 43.
Tebbett, S. B., & Bellwood, D. R. (2021). Algal turf productivity on coral reefs: A meta-analysis. *Marine Environmental Research*, *168*, 105311.
Thacker, R., Nagle, D., & Paul, V. (1997). Effects of repeated exposures to marine cyanobacterial secondary metabolites on feeding by juvenile rabbitfish and parrotfish. *Marine Ecology Progress Series*, *147*, 21–29.
Thacker, R. W., & Paul, V. J. (2001). Are benthic cyanobacteria indicators of nutrient enrichment? Relationship between cyanobacterial abundance and environmental factors on the reef flats of Guam. *Bulletin of Marine Science*, *69*(2), 497–508.
Tovo, A., Menzel, P., Krogh, A., Cosentino Lagomarsino, M., & Suweis, S. (2020). Taxonomic classification method for metagenomics based on core protein families with Core-kaiju. *Nucleic Acids Research*, *48*, e93.
Tribollet, A., Langdon, C., Golubic, S., & Atkinson, M. (2006). Endolithic microflora are major primary producers in dead carbonate substrates of Hawaiian coral reefs. *Journal of Phycology*, *42*, 292–303.
Ullah, H., Nagelkerken, I., Goldenberg, S. U., & Fordham, D. A. (2018). Climate change could drive marine food web collapse through altered trophic flows and cyanobacterial proliferation. *PLoS Biology*, *16*, e2003446.
van den Hoek, C., Cortel-Breeman, A., & Wanders, J. (1975). Algal zonation in the fringing coral reef of Curaçao, Netherlands Antilles, in relation to zonation of corals and gorgonians. *Aquatic Botany*, *1*, 269–308.
Wang, Q., Garrity, G. M., Tiedje, J. M., & Cole, J. R. (2007). Naïve Bayesian classifier for rapid assignment of rRNA sequences into the new bacterial taxonomy. *Applied and Environmental Microbiology*, *73*, 5261–5267.
Webb, A. E., de Bakker, D. M., Soetaert, K., da Costa, T., van Heuven, S. M. A. C., van Duyl, F. C., Reichart, G.-J., & de Nooijer, L. J. (2021). Quantifying functional consequences of habitat degradation on a Caribbean coral reef. *Biogeosciences*, *18*, 6501–6516.

Wu, Y.-W., Simmons, B. A., & Singer, S. W. (2016). MaxBin 2.0: An automated binning algorithm to recover genomes from multiple metagenomic datasets. *Bioinformatics*, *32*, 605–607.

SUPPORTING INFORMATION

Additional supporting information can be found online in the Supporting Information section at the end of this article.

Appendix S1: Contains Figures S1-S8 and Tables S1-S6.

How to cite this article: Cissell, E. C., & McCoy, S. J. (2024). Convergent photophysiology and prokaryotic assemblage structure in epilithic cyanobacterial tufts and algal turf communities. *Journal of Phycology*, *60*, 343–362. https://doi.org/10.1111/jpy.13424